Unveiling the core of the Globular Cluster M 15 in the Ultraviolet[1]

A. Dieball, C. Knigge

Department of Physics and Astronomy, University Southampton, SO17 1BJ, UK

D. R. Zurek, M. M. Shara

Department of Astrophysics, American Museum of Natural History, New York, NY 10024

K. S. Long

Space Telescope Science Institute, Baltimore, MD 21218

P. A. Charles

South African Astronomical Observatory, PO Box 9, Observatory, 7935, South Africa

and

D. Hannikainen

University of Helsinki, P.O. Box 14, SF-00014 Helsinki, Finland

ABSTRACT

We have obtained deep FUV and NUV images of the inner region of the dense globular cluster M 15 with the HST ACS. The FUV–NUV colour-magnitude diagram shows a well-defined track of horizontal branch stars, as well as a trail of blue stragglers and white dwarfs. The main-sequence turnoff is clearly visible at FUV $\simeq$ 23.5 mag and FUV–NUV$\simeq$ 3 mag, and the main-sequence stars form a prominent track that extends at least 2 mag below the main-sequence turnoff. As such, this is the deepest FUV–NUV colour-magnitude diagram of a globular cluster presented so far. Cataclysmic variable and blue straggler candidates are the most centrally concentrated stellar populations, which might either be an effect of mass segregation or reflect the preferred birthplace in the dense cluster core of such dynamically-formed objects. We find 41 FUV sources that exhibit significant variability. We classify the variables based on an analysis of their UV colours and variability properties. We find four previously known RR Lyrae and 13 further RR Lyrae candidates, one known Cepheid and six further candidates, six cataclysmic variable candidates, one known and one probable SX Phoenicis star, and the well known low-mass X-ray binary AC 211. Our analysis represents

the first detection of SX Phoenicis pulsations in the FUV. We find that Cepheids, RR Lyrae stars and SX Phoenicis exhibit massive variability amplitudes in this wave band (several magnitudes).

Subject headings: globular clusters: individual(M 15) – stars: close binaries – stars: variables – ultraviolet: stars

1. Introduction

Globular clusters (GCs) in the Milky Way are old, gravitationally bound stellar systems. Stellar densities in their cores can be extremely high, reaching up to 10^6 stars/pc^3, hence making them ideal crash-test laboratories for studying the dynamics in such dense environments. Close encounters and even direct collisions with resulting mergers between the cluster stars are inevitable, leading to a variety of dynamically formed, exotic stellar populations like blue stragglers (BSs), cataclysmic variables (CVs), low-mass X-ray binaries (LMXBs), and probably binary horizontal branch (HB) stars and other close binary (CB) systems. CBs are important for our understanding of GC evolution, since the binding energy of a few CBs can rival that of a GC. Thus, by transferring their orbital energy to passing single stars, CBs can significantly affect the dynamical evolution of the cluster (e.g. Elson et al. 1987, Hut et al. 1992, and references therein). This depends critically on the number of CBs; if there are only a few CBs, long-term interactions dominate the cluster evolution, but the presence of many CBs can lead to violent interactions that heat the cluster and cause its expansion and evaporation on significantly shorter time-scales. Therefore, knowledge of the CB populations in the cores of clusters is crucial to understanding the evolution of clusters.

However, despite their impact on cluster evolution and their importance for our understanding of dynamical binary formation and binary evolution, there have been only a few detections of binaries in GCs during the past decades. The study of binaries has been extremely difficult due to the spatial resolutions and detection limits of the available telescopes. Only with the arrival of *Chandra* and the *Hubble Space Telescope (HST)*, with their improved imaging capabilities, has it been possible to finally detect large numbers of CVs and other binary systems (e.g. Grindlay et al. 2001; Edmonds et al. 2003a, 2003b; Knigge et al. 2002, 2003; Dieball et al. 2005a and references therein).

---

[1]Based on observations with the NASA/ESA *Hubble Space Telescope*, obtained at the Space Telescope Science Institute, which is operated by the Association of Universities for Research in Astronomy, Inc., under NASA contract NAS5-26555.

CBs and other dynamically formed systems share an observational characteristic: they show a spectral energy distribution that is bluer than that of other cluster members and emit radiation in the far-ultraviolet (FUV). "Ordinary" stars, like main-sequence (MS) stars and red giants (RGs), are too cool to show up at these wavelengths. As a consequence, crowding is generally not a severe problem in FUV imaging, very much unlike optical imaging, which is often nearly impossible in dense cluster cores. Thus, a deep, high-resolution FUV-survey is the ideal tool to detect and study these stellar species.

So far, deep FUV studies have been carried out in detail only for two clusters: 47 Tuc (Knigge et al. 2002, 2003) and NGC 2808 (Brown et al. 2001; Dieball et al. 2005). In 47 Tuc, Knigge et al. (2002) found FUV counterparts to all of the *Chandra* CV candidates known at that time in the core of this cluster (Grindlay et al. 2001)[2] and confirmed their CV nature. In addition, several additional CV candidates were suggested, and a clean, well-populated FUV BS sequence and numerous young white dwarfs (WDs) on the upper end of the cooling sequence were found. In NGC 2808, Brown et al. (2001) used FUV and NUV imaging to uncover a population of sub-luminous hot HB stars that probably underwent a late helium-core flash on the WD cooling curve. Our own reanalysis of this data set pushed the detection limits deeper and revealed numerous BSs, CV candidates, and hot young WDs in this cluster (Dieball et al. 2005a).

M 15 is one of the oldest (13.2 Gyr; McNamara et al. 2004) low-metallicity ([Fe/H] = −2.26; Harris 1996) GCs in our Galaxy, at a distance of 10.3 kpc (van den Bosch et al. 2006). It has received considerable attention in the literature for numerous reasons. It is probably a core-collapsed cluster, with a very small and very dense core ($R_c \approx 0\farcs07$, $\rho_c \approx 7\times10^6 M_\odot \mathrm{pc}^{-3}$; van den Bosch et al. 2006). Because of its unusual compact core, high central velocity dispersion, and luminosity profile, it has even been suggested that M 15 hosts an intermediate-mass black hole (IMBH) of up to a few thousand solar masses (e.g. Peterson et al. 1989; Guhathakurta et al. 1996; Gebhardt et al. 1997; Gerssen et al. 2002). However, Baumgardt et al. (2003) presented N-body models that are capable of explaining the observed velocity dispersion and luminosity profile without the need for a central IMBH, but with a concentration of neutron stars (NSs) and massive WDs in the centre due to mass segregation. McNamara et al. (2003) also found that there is little evidence for an IMBH, their proper-motion dispersion profile of the inner region of M 15 being in good agreement with the predictions from Baumgardt et al. (2003). Most recently, van den Bosch et al. (2006) suggested a mass of 3400 $M_\odot$ in the central 0.05 pc, which could either be an IMBH, or a

[2]Note that recently Heinke et al. (2005) published a catalog of X-ray sources of 47 Tuc comprising 300 objects within one half-mass radius. Work is in progress to identify counterparts to all the sources located within the FUV field of view (C. Knigge 2006, private communication).

large number of compact objects, or a combination of both.

M 15 is also the only Galactic GC known to harbour *two* bright LMXBs. The first one, 4U 2127+119, was identified by Aurière et al. (1984) with the optical counterpart AC 211. It has an orbital period of 17.1 hr (Ilovaisky et al. 1993) and is one of the optically brightest LMXBs known. Its high $L_{\rm opt}/L_{\rm X}$ ratio suggests that the system is an accretion disk corona source. White & Angelini (2001) used *Chandra* observations to resolve 4U 2127+119 into *two* X-ray sources, separated by just 2.″7 (see also Charles et al. 2002; Hannikainen et al. 2005). One of these was the previously known LMXB AC 211. The second source, CXO J212958.1+121002 or M 15 X-2, is actually 2.5 times brighter than AC 211 in X-rays and is the likely source of the X-ray bursts observed in 1988 and 2000 (Dotani et al. 1990; Smale 2001). Its optical counterpart is a blue $U \approx 19$ mag star (star 590 in De Marchi & Paresce 1994). Dieball et al. (2005b) found that M 15 X-2 is an ultra-compact X-ray binary (UCXB) with an orbital period of 22.6 minutes, only the third confirmed such object in a GC.

M 15 is one of the three original Oosterhoff type II clusters identified in Oosterhoff (1939). More than 200 variable stars are known in this cluster; the majority of them are RR Lyrae stars (e.g. Silbermann & Smith 1995; Clement et al. 2001; Arellano et al. 2006). Clement et al. (2001) list 204 entries in their catalog of variable stars in M 15, out of which 149 are RR Lyrae stars (at least 55 are of type RRab, 52 of type RRc, and 23 of type RRd). Tuairisg et al. (2003) classified 19 RRc (10 new ones), 12 RRab (six previously unknown) and two RRd (one previously unknown). However, the classification of the RR Lyrae subtype is not always consistent with Clement et al. (2001).

The cluster also hosts other interesting stellar populations, among them a large number of BSs (e.g. Yanni et al. 1994). At least three SX Phoenicis stars (Jeon et al. 2001; Kravtsov & Zheleznyak 2003), eight millisecond pulsars (Phinney 1996) and three dwarf nova (DN) candidates are known (Shara et al. 2004; Hannikainen et al. 2005). De Marchi & Paresce (1994, 1996) also found extreme blue stars in their broadband UV colour-magnitude diagram (CMD), which were explained by D'Antona et al. (1995) as the merger product of two low-mass helium white dwarfs. Most of the above mentioned exotica are indicators of strong dynamical interaction. M 15's optical CMD (Van der Marel et al. 2002) shows a prominent blue horizontal branch (BHB) and extreme blue horizontal branch (EHB) stars with a few gaps along the HB (see below our Fig. 4, right panel).

Here we present FUV and NUV data of M 15 taken with the Advanced Camera for Surveys (ACS) on board the *HST*. In Sect. 2 we describe the data and their reduction. We present the analysis of the photometry and the FUV versus NUV CMD in Sect. 3. Our search for variability among our catalog stars and a study of the variable sources are given

in Sect. 4. Our results are summarized in Sect. 5.

2. Observations and data reduction

M15 was observed with the ACS onboard *HST* for a total of 10 orbits in 2003 October and 2004 October to December. The observations were spaced out through this period in order to improve our chances of measuring time-variable phenomena. On the first visit in 2003 October, eight images with individual exposures of 290 s were obtained using the NUV F220W filter in the High Resolution Channel (HRC). The remaining visits were used to obtain a total of 90 images using the FUV F140LP filter in the Solar Blind Channel (SBC). Each of the SBC visit consisted of eight 300 s exposures, followed by either a 40 s or a 140 s exposure at the end of the visit. The same pointing and no dither pattern was used for all of the observations. An observing log can be found in Table 1. The pixel sizes are $0\farcs034 \times 0\farcs030$ for the SBC, resulting in a nominal field of view of $35'' \times 31''$, and $0\farcs028 \times 0\farcs025$ pixels for the HRC, covering a nominal $29'' \times 26''$ field of view.

As the ACS focal surfaces are inclined towards the principal rays, the resulting exposures are geometrically distorted. This distortion consists of two effects, namely, a tilted elongation of the ACS apertures, causing the pixel scale to be smaller along the radial direction than along the tangential direction of the Optical Telescope Assembly field of view, and a variation of pixel area across the detector. In order to correct these effects, each pixel of the distorted original image has to be mapped onto pixels in a rectified, undistorted output image, taking into account shifts and rotations between images and the - known - optical distortion of the camera. For a detailed discussion on the distortion effects of ACS imaging and the use of `multidrizzle` we refer the reader to the *HST* ACS data handbook and references therein.

We created master images for each filter using `multidrizzle` running under `PyRAF`. As a first step, we geometrically corrected the single flat-fielded images. To account for small shifts between the desired and actual pointing positions, we used the `IRAF`[3] tasks `crossdriz` and `shiftfind` on the single drizzled (i.e. geometrically corrected) images. The shifts are usually less than a pixel but can be as high as 1.8 pixels for one orbit in SBC/F140LP. For the HRC/F220W images we found that it is sufficient to use the pipeline combined and drizzled image that is created for each orbit. Note that the combined and geometrically corrected ACS/SBC and HRC images produced by `multidrizzle` have a pixel scale of $0.025''$/pixel

[3]`IRAF` (Image Reduction and Analysis Facility) is distributed by the National Astronomy and Optical Observatory, which is operated by AURA, Inc., under cooperative agreement with the National Science Foundation.

Table 1: Observation log. Col. (1): Visit. Col. (2): Data set. Col. (3): Start date of the observations. Col. (4): Total exposure time for that data set. Cols. (5) and (6): Detector and Filter, respectively. See text for details.

visit	dataset	start date	total exp.time	detector (ACS)	filter
1	J8SI08010	2003-10-27 02:03:00	2320	HRC	F220W
2	J8SI01011	2004-10-14 05:44:00	2400	SBC	F140LP
2	J8SI01RKQ	2004-10-14 06:29:00	40	SBC	F140LP
3	J8SI01021	2004-10-14 07:15:00	2400	SBC	F140LP
3	J8SI01S8Q	2004-10-14 08:00:00	140	SBC	F140LP
4	J8SI01031	2004-10-14 08:51:00	2400	SBC	F140LP
4	J8SI01SIQ	2004-10-14 09:36:00	140	SBC	F140LP
5	J8SI01041	2004-10-14 10:27:00	2400	SBC	F140LP
5	J8SI01T4Q	2004-10-14 11:12:00	140	SBC	F140LP
6	J8SI01051	2004-10-14 12:03:00	2400	SBC	F140LP
6	J8SI01TEQ	2004-10-14 12:48:00	140	SBC	F140LP
7	J8SI02011	2004-10-24 10:27:00	2400	SBC	F140LP
7	J8SI02LTQ	2004-10-24 11:13:00	40	SBC	F140LP
8	J8SI03011	2004-11-06 19:55:00	2400	SBC	F140LP
8	J8SI03GCQ	2004-11-06 20:40:00	40	SBC	F140LP
9	J8SI04011	2004-11-17 11:49:00	2400	SBC	F140LP
9	J8SI04JDQ	2004-11-17 12:34:00	40	SBC	F140LP
10	J8SI05011	2004-11-26 16:30:00	2400	SBC	F140LP
10	J8SI05YYQ	2004-11-26 17:16:00	40	SBC	F140LP
11	J8SI06011	2004-12-05 03:36:00	2400	SBC	F140LP
11	J8SI06BSQ	2004-12-05 04:22:00	40	SBC	F140LP

and are normalized to 1 s exposure time. The total exposure times are 24800 s for the FUV and 2320 s for the NUV master image and have to be considered when calculating the photometric errors. The combined and geometrically corrected FUV (SBC/F140LP) and NUV (HRC/F220W) master images are shown in Fig. 1 and 2, respectively. As expected, the FUV image is considerably less crowded than the NUV image. Both images show significant concentrations of sources towards the cluster core.

2.1. Source detection

As one of our main goals of this study is to construct a deep FUV–NUV CMD, we took special care to identify as many of the weak sources as possible. We first used `daofind` (Stetson 1991) running under `IRAF` to create an initial list of source detections. After some experimentation, we used an FWHM of 5 pixels and a rather high threshold to maximize the number of faint sources detected and minimize the number of multiple detections in and around bright sources. We caution that the FWHM used in `daofind` does not reflect the "true" FWHM of the SBC point-spread-function (PSF), but is rather a compromise to minimize the number of false detections at the image rims and in the defect or shaded areas of the MAMA detectors (due to the broken anode of the ACS MAMA; see the ACS handbook for details). We overplotted the source coordinates on the FUV master image and inspected them by eye. Overall, the process worked well. However, we found that the automatic process left some faint sources missing and others (bright sources) that were multiply detected. We inserted missing faint sources by hand and deleted false detections at the rims of the image, in the defect area, and multiple detections around bright stars. In the end, our resulting catalog of FUV sources contained 2731 entries.

Source detection in the NUV master image worked well with standard values for the threshold (Stetson 1991), and 9164 sources were detected. In order to match the FUV and NUV catalogs, we first transformed the FUV coordinates onto the NUV frame using the `geomap` and `geoxytran` tasks running under `IRAF`. We used 30 bright stars that are common in both the FUV and NUV image as a reference list required by `geomap` to determine the geometrical transformation between the two frames. Small shifts between the transformed FUV and the NUV coordinate of sources common in both frames are to be expected. These shifts depend on how well the applied coordinate transformation actually worked, and also on the width of the stars' PSF in the images. We thus checked for common pairs within a tolerance of 1.5 pixels, which resulted in 1686 matches. Increasing the tolerance to 2.5 pixels added another 193 matches. These additional matches are uniformly distributed across the NUV master image with no preferred location, suggesting that our coordinate transformation

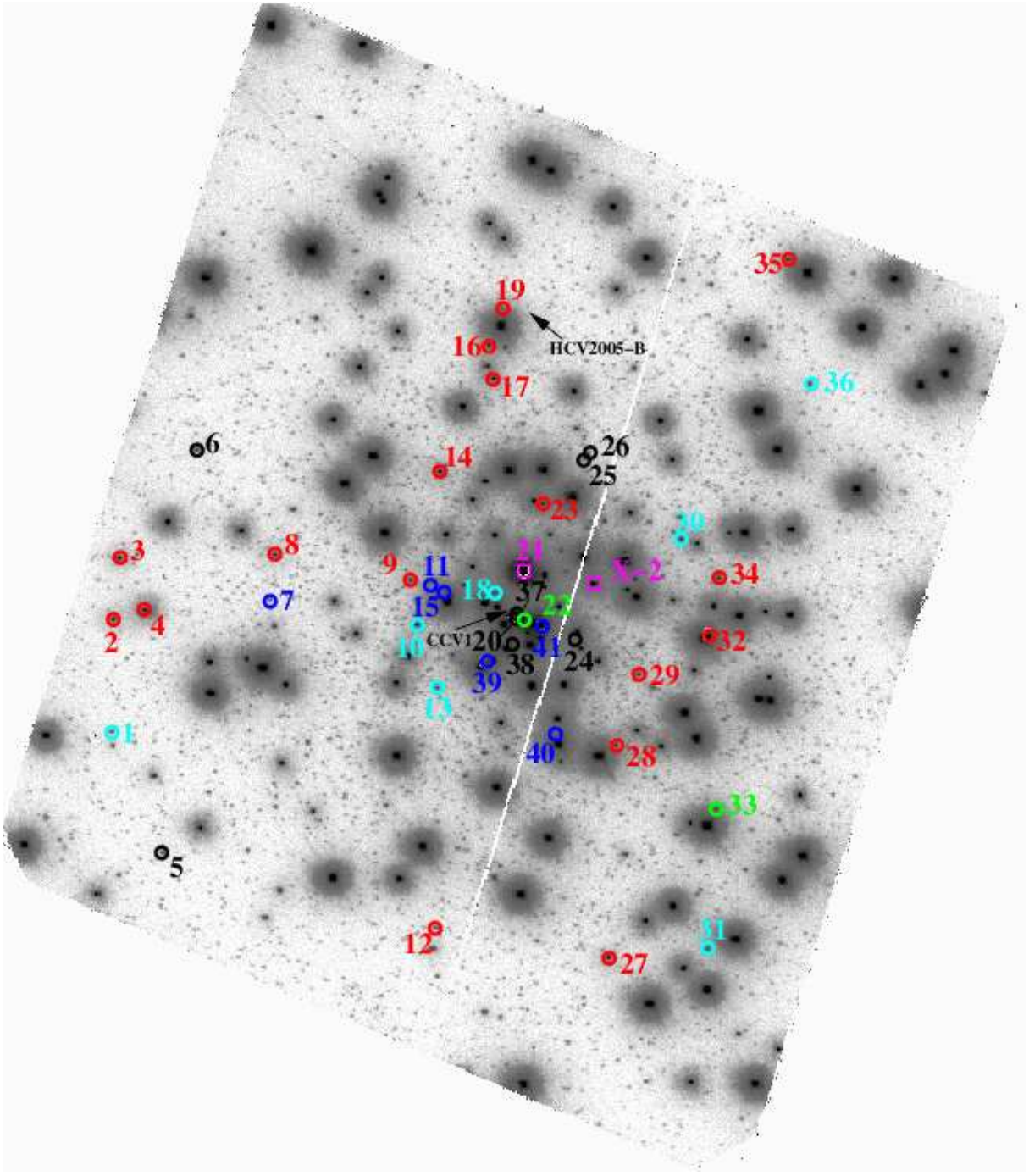

Fig. 1.— Combined and geometrically corrected master image of all FUV SBC/F140LP exposures taken from the central region of M 15. North is up and east to the left. The pixel scale is $0\farcs025$ pixel^{-1}, and the field of view is $35'' \times 31''$. Variables are marked with circles and their number given in Tables 4 and 5. The colours denote: red - RR Lyrae and candidates, blue - CV candidates, green - SX Phoenicis and candidates, cyan - Cepheid and candidates, magenta squares - LMXBs, black - other variables. The locations of two further X-ray sources, HCV 2005-A and HCV 2005-B, which are situated in our field of view and are suspected DNe, are indicated with arrows. Note that their FUV counterparts are too faint to show up in our FUV master image, but the sources could be identified in the NUV. See Sect. 4.4 for details.

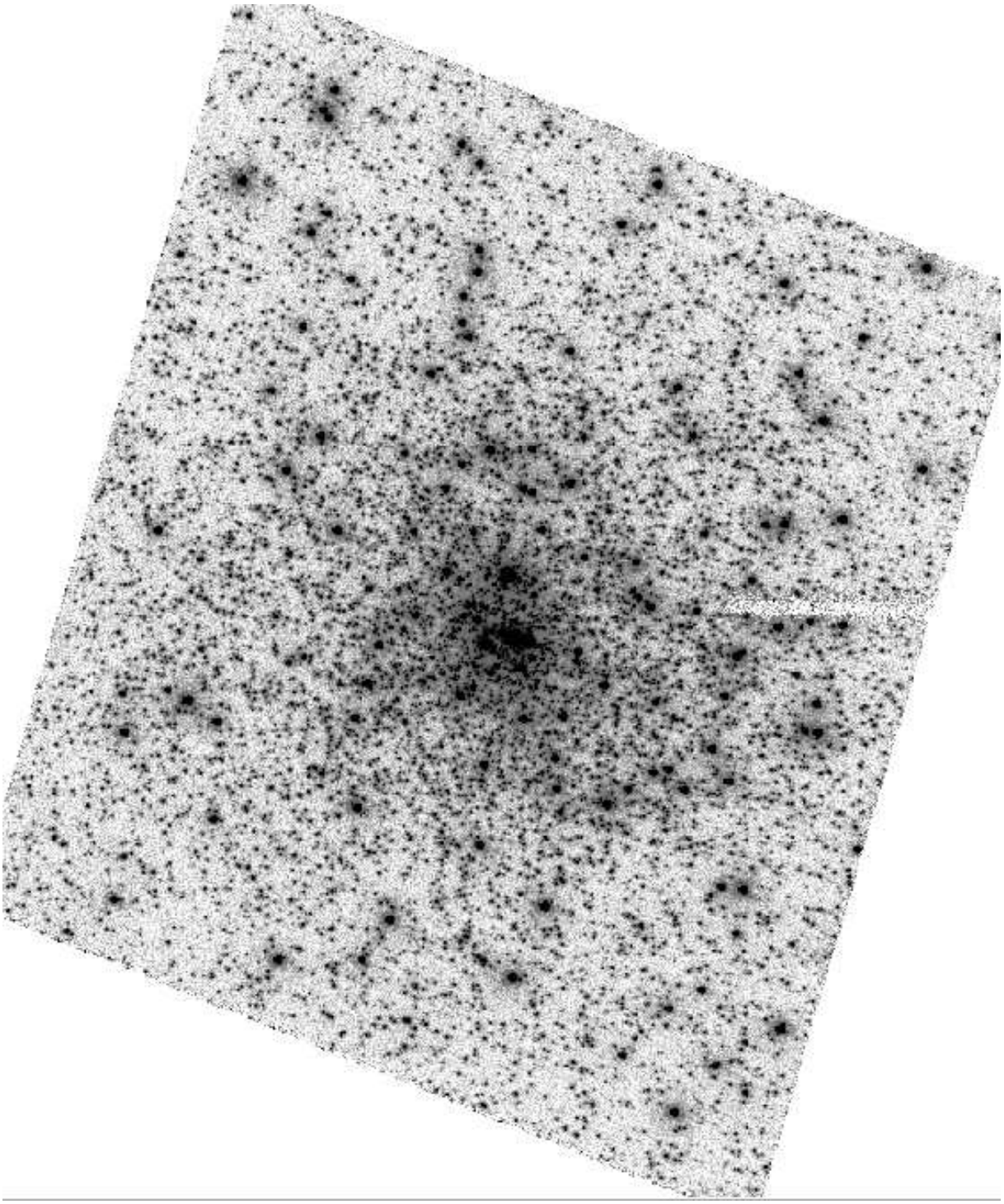

Fig. 2.— Master image of all NUV exposures of the same region of M 15. The orientation is the same as in Fig. 1. Both Fig. 1 and 2 are displayed on a logarithmic intensity scale in order to bring out the fainter sources.

worked very well and no distortions are visible. A total of 2137 FUV sources are located within the NUV field of view. Out of these, 258 objects were not matched with an NUV counterpart. Inspecting these unmatched sources by eye, we added further 34 NUV sources to our initial NUV source list. Photometry on these 34 additional NUV sources was then performed without a Gaussian recentering as these additional sources are very faint and a recentering algorithm will actually centre on the next brighter star, see Sect. 2.2 and 4. Counterparts to the remaining 224 unmatched FUV sources are too faint to show up in the NUV master image.

We expect that a few false matches are among our FUV–NUV pairs. The number of false matches depends on the number of objects in the two source lists, the number of found pairs, and the matching tolerance (here we chose 2.5 pixels). Following Knigge et al. (2002), we estimate that less than ≈ 37 pairs (1.9% of all found matches) are chance coincidences due to the source density in the NUV field of view. Most of the remaining unmatched FUV sources are located outside or at the rim of the NUV frame.

We chose 2.5 pixels as our maximum tolerance radius as a compromise in order to get all common pairs, but to keep the number of false matches at an acceptable level. As can be seen from Table 2, the actual matching radius is in most cases much smaller, with a mean matching radius of just 0.5 pixels.

A catalog listing all our FUV–NUV matches is available in the electronic edition of the Journal. For reference, Table 2 lists only 10 entries. We also include sources without NUV counterparts in our catalog because these are likely to include additional WD and CV candidates.

2.2. Aperture photometry

Photometry was carried out on the combined and geometrically corrected images for each filter using `daophot` (Stetson 1991) running under `IRAF`. We used apertures of 3 pixels for both the FUV and the NUV data and allowed also for a Gaussian recentering of the input coordinates derived in `daofind`. In the FUV, aperture corrections were determined via curves of growth constructed from isolated stars in our master images. For the NUV data, we used the encircled energy fractions published by Sirianni et al. (2005). Because of close neighbour stars in the centre of M 15 (especially important in the HRC/F220W images; see Fig. 2), we chose a small sky annulus of 5 – 7 pixels to minimize the number of stars within the sky annulus. However, our small sky annulus also contains flux from the target star. Thus, too much flux will be subtracted during sky subtraction. For a few isolated stars, we

Table 2. Catalog of all sources in our FUV field of view. The first nine columns are self explanatory. The tenth column denotes the matching radius between the NUV and transformed FUV Cartesian coordinates. The radius from the cluster centre (at x≈900 and y≈850 in our FUV master image, determined from star number counts in both master images) is given in column eleven. The optical B, V, U magnitudes and the corresponding ID from the Van der Marel et al. (2002) optical catalog are given in the last four columns. An asterisk means that there is no entry because there is no match with an NUV source and/or with an optical source. Only entries 1 – 5 and 1000 – 1005 are given. Table 2 is published in its entirety in the electronic edition of the *Astrophysical Journal*. A portion is shown here for guidance regarding its form and content.

id	alpha [h m s]	delta [° ′ ″]	x_{FUV} [pixel]	y_{FUV} [pixel]	FUV [mag]	ΔFUV [mag]	$FUV - NUV$ [mag]	$\Delta(FUV - NUV)$ [mag]	tolerance [pixel]	radius [″]	V [mag]	B [mag]	U [mag]	id_{VDM}
1	21 29 59.519	12 9 51.352	164.820	516.783	15.892	0.003	*	*	*	20.179	*	*	*	*
2	21 29 59.514	12 9 53.303	167.642	594.829	24.823	0.116	*	*	*	19.388	*	*	*	*
3	21 29 59.507	12 9 53.013	171.709	583.227	25.584	0.178	*	*	*	19.390	20.125	20.674	20.576	25120
4	21 29 59.503	12 9 53.360	174.173	597.098	23.667	0.058	*	*	*	19.216	*	*	*	*
5	21 29 59.502	12 9 54.293	174.907	634.400	24.352	0.084	*	*	*	18.912	18.659	19.282	19.174	24915
1000	21 29 58.603	12 9 46.293	702.035	314.413	23.500	0.049	*	*	*	14.275	*	*	*	*
1001	21 29 58.602	12 9 45.692	702.384	290.392	23.018	0.039	*	*	*	14.837	18.232	18.775	18.636	8759
1002	21 29 58.602	12 9 56.222	702.513	711.564	23.993	0.072	3.154	0.080	0.690	6.029	19.673	20.072	20.012	5498
1003	21 29 58.602	12 10 12.702	702.642	1370.79	17.520	0.005	-0.204	0.007	0.072	13.923	*	*	*	*
1004	21 29 58.601	12 9 52.474	702.917	561.646	23.815	0.067	*	*	*	8.732	*	*	*	*
1005	21 29 58.601	12 9 56.542	703.298	724.359	23.182	0.051	2.973	0.058	0.350	5.835	18.920	19.424	19.271	5396

were able to choose a larger sky annulus of 50 – 60 pixels. Assuming that we get the "true" flux for the source we want to measure if we use the larger sky annulus, we can then apply a flux correction for the small sky annulus to all sources. These flux corrections depend on the PSF of the star, which is different for the SBC/F140LP and HRC/F220W. For the sake of simplicity, we assume the corrections to be the same for all stars in the master image in each filter. Table 3 lists all encircled energy fractions and sky corrections for apertures of 1 – 10 pixels for both the SBC/F140LP and HRC/F220W filters.

In order to convert count rates into fluxes and STMAGs, we used conversion factors of

$$\mathrm{PHOTFLAM_{SBC/F140LP}} = 2.7182 \times 10^{-17} \mathrm{erg\,cm^2 \AA^{-1} counts^{-1}}$$
$$\mathrm{PHOTFLAM_{HRC/F220W}} = 7.9999 \times 10^{-18} \mathrm{erg\,cm^2 \AA^{-1} counts^{-1}}$$

Fluxes are then converted into STMAGs using

$$\mathrm{STMAG} = -2.5 \times \log_{10}(\mathrm{flux}/(\mathrm{ee} \times \mathrm{skycorr})) + 21.1,$$

where flux = countrate × PHOTFLAM (i.e. the measured flux inside our chosen aperture), ee is the encircled energy fraction and skycorr is the flux correction for the small sky annulus listed in Table 3. The conversion factors PHOTFLAM are given in the image headers; see also the ACS data handbook.

3. The FUV–NUV CMD

The FUV–NUV CMD of the core region of M 15 is shown in Fig. 3. Several stellar populations show up, such as the bright HB stars, BSs, and WD candidates. A number of sources are located between the WD cooling sequence and the MS. These sources include both detached and interacting WD-MS binaries, and we refer to these sources as "gap objects", see Sect. 3.4. The region of data points in the lower right (i.e. faint and red) part of the CMD denotes the MS stars and RGs. The turnoff is at FUV ≈ 23.5 mag and FUV–NUV ≈ 3 mag at the bright end of this data region. As can be seen, our CMD reaches at least 2 mag below the FUV MS turnoff. A trail of stars extends from the MS turnoff towards red and fainter magnitudes. Sources that match with optical RGs are all located on this trail. Error bars for each data point are also plotted.

For orientation purposes, we have also calculated and plotted a set of theoretical tracks representing the zero-age main-sequence (ZAMS), the zero-age horizontal branch (ZAHB), and the WD cooling sequence. The sequences were constructed using theoretical ZAHB models from Dorman (1992), the fitting formulae of Tout et al. (1996), and the Wood

(1995) grid of theoretical WD cooling curves for our WD cooling sequence. We then used SYNPHOT within STSDAS to calculate the FUV and NUV magnitudes of stars on the corresponding sequence. This was achieved by interpolating on the Kurucz grid of model stellar atmospheres and folding the resulting synthetic spectra through the response of the appropriate filter+detector combinations. For the WD cooling sequence, we used a grid of synthetic DA WD spectra kindly provided by Boris Gänsicke (see Gänsicke et al. 1995). The procedure is described in more detail in Dieball et al. (2005a). For all our synthetic tracks we adopted a distance of 10.3 kpc, a reddening of $E_{B-V} = 0.1$, and a cluster metallicity of $[Fe/H] = -2.26$ (Harris 1996).

In the following, we describe the stellar populations within our CMD in more detail.

3.1. HB stars

M 15 is one of the most metal-poor GCs in our Galaxy. Like other metal-poor GCs, its optical CMD reveals a blue HB and a prominent blue tail extending to fainter magnitudes (Van der Marel et al. 2002; see also Fig. 4). This tail is the so-called EHB, which is separated from the horizontal part by a gap. Brown et al. (2001) suggested that the subluminous EHB stars in NGC 2808 (as well as the EHB gap in its optical CMD) can be explained by a late helium-core flash that these stars undergo while they descend the WD sequence. In NGC 2808's FUV–NUV CMD, the HB stars cluster in two distinct data clumps around FUV–NUV ≈ -0.7 mag (BHB) and FUV–NUV ≈ -1.2 mag (EHB).

Our FUV–NUV CMD of M 15 reveals a strong population of 133 HB stars along a well-defined HB sequence and within a bright data region at FUV ≈ 15.5 mag and FUV–NUV ≈ -0.6 mag. This is different from the FUV–NUV CMD of NGC 2808 (Brown et al. 2001; Dieball et al. 2005a), which shows two distinct clumps of HB stars, corresponding to the optical EHB and BHB. However, our HB stars within the bright data clump match with optical EHB stars, whereas the sources along the ZAHB match with BHB stars, see Sect. 3.5 and Fig. 4 below. Thus, we possibly see a similar population of EHB stars here as in NGC 2808.

3.2. Blue Stragglers

BSs are thought to be the end product of a collision or coalescence of two or more MS stars; i.e., they are dynamically formed objects and as such are expected to be preferentially found in the dense cluster cores. As they are more massive than ordinary cluster MS stars,

we expect them to be slightly evolved. In optical CMDs, they are therefore located above and slightly to the red of the MS. In our FUV–NUV CMD, see Fig. 3, we see a trail of stars starting from the clump of MS stars and RGs in the lower right corner and reaching along the ZAMS up towards the clump of EHB stars at FUV $\approx$ 15.5 mag. This trail of stars is below the ZAHB and less clearly defined than the sequence formed by the HB stars. The location of these sources roughly agrees with the expected location of BSs, i.e. along the ZAMS but brighter than the MS turnoff. We find 69 BS candidates but caution that a small number of these may not be BSs since the various stellar populations in our CMD partly overlap. The discrimination between the gap objects and BS candidates is particularly difficult and would require further observations.

3.3. White Dwarfs

A population of about 28 sources can be seen in Fig. 3 that lie along or close to the theoretical WD cooling curve and are therefore probably hot, young WDs. Twenty-five of our WD candidates are brighter than 22.5 mag.

Following Knigge et al. (2002), we can estimate the number of expected WDs by scaling from the number of HB stars in the same field of view. We count $\approx$ 133 BHB and EHB stars in our CMD. Given that the lifetime of stars on the HB is approximately $\tau_{HB} \simeq 10^8$ yr (e.g. Dorman 1992), we can predict the number of WDs above a given temperature on the cooling curve from the relation

$$\frac{N_{WD}}{N_{HB}} \sim \frac{\tau_{WD}}{\tau_{HB}}$$

where τ_{WD} is the WD cooling age at that temperature (e.g. Knigge et al. 2002). WDs at FUV $\sim$ 22.5 mag on our WD sequence have a temperature of $T_{eff} = 26,000$ K and a corresponding cooling age of $\tau_{WD} \simeq 3.99 \times 10^7$ yr. We therefore predict a population of approximately 53 WDs brighter than FUV = 22.5, which strongly suggests that most if not all of our candidates are indeed WDs. Note that more and possibly fainter WDs are present in our FUV field of view but are not detected in the NUV and thus do not appear in our FUV–NUV CMD.

We caution that this is a simplistic approach and we do not take the effects of mass segregation into account. Richer et al. (1997) suggested that if the WD cooling times are an appreciable fraction of the cluster age (or rather the relaxation time), the slope of the cluster initial mass function and the relation between stellar mass and MS lifetime become important. This can increase the expected number of faint WDs up to a factor of 3.

3.4. CV candidates

As can be seen from our Fig. 3, there are a number of sources that are located between the WD cooling sequence and the ZAMS. This is a region in the CMD where we expect to find CVs, but also detached WD-MS binaries. As we cannot discriminate between true CVs and detached WD-MS binaries based on our FUV–NUV CMD alone, we refer to these sources as "gap objects", thus denoting sources that are located in the gap region between the WD cooling sequence and the MS. We find ≈ 57 sources in this gap zone but caution again that this figure is not to be taken as a strict number as the discrimination especially between these gap objects and other populations like WDs, MS stars and BSs is somewhat difficult. In the following, we compare this number with theoretical predictions for CVs. For this purpose, we scale the predicted number of dynamically-formed CVs in 47 Tuc to M 15.

For 47 Tuc, Di Stefano & Rappaport (1994) predicted a population of ~ 190 active CVs formed via tidal capture. Ivanova et al. (2006) investigated all sorts of dynamical and primordial formation channels and predict a few hundred CVs that should be present in the cluster core in 47 Tuc. However, Shara & Hurley (2006) found that dynamically produced CVs have shorter lives than their field counterparts, which decreases the expected number of CVs by a factor of 3. They based their study on N-body simulations starting with 100,000 objects and a binary fraction of 5% and found that exchange interactions are more likely to make CVs with higher mass MS donors (donor mass $> 0.7 M_{\odot}$), which are more likely to be short-lived than their field counterparts.

We follow the simplified estimate for the capture rate in GC cores (Heinke et al. 2003),

$$\Gamma \propto \rho_c^{1.5} \cdot r_c^2,$$

where ρ_c is the central luminosity density and r_c is the core radius. Taking ρ_c, r_c, and the distance to the clusters from Harris (1996), we find that the expected number of dynamically-formed CVs in M 15 is ≈ 200, comparable to what is expected for 47 Tuc. Di Stefano & Rappaport (1994) found that approximately half of the captures would take place within 1 core radius. Given our detection limits, we cannot hope to detect the very oldest and faintest CVs. The coolest WDs that we detect have $T_{eff} = 26,000$ K (see Sect. 3.3). This suggests that we can only expect to find relatively bright, long-period CVs above the period gap (see Townsley & Bildsten, 2003, their Figs. 1 and 2). About 20 of these long-period CVs should exist in 47 Tuc (Di Stefano & Rappaport, 1994, their Fig. 3 and Table 5). Scaling this number, we expect 21 such systems in M 15. As our image covers more than $5 \times r_{core}$, we expect to find most, but perhaps not all, of these sources. As a rough estimate, we suggest that 10 – 21 of the long-period, active CVs should be within our field of view. If dynamical effects shorten the lifetime of CVs by a factor of about 3, as suggested by

Shara & Hurley (2006), the expected number of CVs in our data would drop accordingly. We caution that these are extremely rough estimates, but they suggest that some, but not all, of our gap objects are likely to be CVs.

3.5. Optical counterparts

An optical catalog of 31,983 sources in the central region of M 15 was presented by Van der Marel et al. (2002). These data were obtained in 1994 April in the context of *HST* program GO-5324, using the WFPC2/F336W, F439W, and F555W camera/filter combination, with the PC centred on the cluster centre. The chosen WFPC2 filters correspond roughly to the Johnson U, B, and V bands. First results from these observations were reported by Guhathakurta et al. (1996). Van der Marel et al. (2002) applied an improved astrometric and photometric calibration to the original star list, and we used this catalog to find optical counterparts for our FUV sources.

We first transformed the α, δ coordinates in the optical catalog to the Cartesian (x, y) FUV coordinate system, using the `IRAF` task `wcsctran`. Note that since the optical α, δ coordinates do not correspond exactly to the FUV ones, the Cartesian coordinates also do not match exactly and require a further transformation. Thus, we selected 80 HB stars that are common to both catalogs and could be easily identified. These 80 sources served as our reference list for a coordinate transformation. Using the `IRAF` tasks `geomap` and `geoxytran`, we transformed the physical FUV coordinate system to the optical (x, y) one.[4] Allowing for a matching radius of 1.5 pixel, we then found 1632 sources that are common to both the optical and our FUV catalog.

We checked the location of the common sources in both the FUV–NUV and the optical CMD and found that indeed all stellar populations are at their expected location in the optical CMD, i.e. our matched HB stars are on the optical blue or extended blue horizontal branch (see Sect. 3.1), and the matched sources within our BS region are in the BS region

[4]We found a rather large shift between our FUV and the optical coordinates given in the electronic version of the optical catalog available via CDS, Strasbourg. For example, the coordinates for the well-known LMXB AC 211 (optical id 5435) are $21^h29^m57.91^s + 12°10'06\farcs8$ in the VizieR version of the optical catalog. In our catalog presented in Table 2, AC 211 (FUV ID 1580) is at $21^h29^m58.238^s + 12°10'1\farcs65$, which is much closer to previously published figures (White & Angelini 2001; Kulkarni et al. 1990). However, the original electronic table in Van der Marel et al. (2002) listed only $\Delta\alpha$ and $\Delta\delta$ with respect to cluster centre and no absolute α, δ. Applying $\Delta\alpha$ and $\Delta\delta$ to the cluster centre coordinates given in Van der Marel et al. (2002) results in $21^h29^m57.965^s + 12°10'02\farcs85$ for AC 211, closer to previous published values and different from the coordinates computed by VizieR.

in the optical CMD, and so on. This is illustrated in Fig. 4, where we indicate the different stellar populations found in our FUV–NUV CMD with different colours and overplotted them on the optical CMD. A few BSs are within the optical MS region, which indicates that these BSs are formed from the coalescence of lower mass MS stars and thus are of a lower mass than the BS above the optical MS turnoff. All matched sources that are located in the MS/RG clump in our FUV–NUV CMD correspond to optical MS stars or RGs. We did not find any counterparts to our WD candidates, which is to be expected as WDs are extremely faint in the optical. We found 12 matches among our gap objects. Ten of these are located along the optical MS. These systems might be CVs or detached WD-MS binaries that are dominated by the MS star in the optical, whereas the systems are dominated by the accretion disk or a hot WD in the FUV. Note that the gap object with the bluest optical counterpart is actually the UCXB M 15 X-2.

3.6. Radial distributions of the stellar populations

Fig. 5 shows the cumulative radial distribution of the stellar populations that show up in our CMD and that are discussed above. As our CMD is limited by our NUV data, we only consider data that are brighter than NUV = 21 mag. We note that the radial distribution of MS stars is not shown because the difference between the MS stars and all other populations might be an effect of incompleteness in the cluster core in the FUV image. A few bright stars are concentrated in the cluster centre, and the broad PSF wings of the bright sources hamper the detection of faint objects, especially MS stars and WDs. As only two WD candidates with NUV ¡ 21 mag are present in our limited data set, we show only the radial distributions of BS candidates, gap objects, and HB stars, see the top panel in Fig. 5. All of the gap sources are CV candidates to start with, but we caution again that this sample might also contain detached WD-MS binary candidates. The gap objects seem to be the most centrally concentrated stellar population, followed by BS candidates and then HB stars.

We applied a Kolmogorov-Smirnov (K-S) test on the restricted data set in order to determine the statistical significance of the differences between the various stellar populations. However, we caution that HB stars, gap sources, and BS candidates cannot be clearly distinguished based on the CMD alone, and we might have sources in one sample that actually belong to another. Our selected data set contains 133 HB stars, 69 BS candidates, and 16 gap sources.

The K-S test returns the probability that the maximum difference between the two distributions being compared should be as large as observed, under the null hypothesis that the distributions are drawn from the same parent populations. In this sense, a high K-S

probability agrees with both distributions to be likely from the same parent distribution. The smaller the returned K-S probability, the more unlikely it is that they originate from the same parent distribution, i.e. the more different are the two compared distributions. BS candidates and gap sources differ from the HB population with K-S test probabilities of 14% (BSs vs. HBs) and 2% (gap sources vs. HBs). Gap objects and BS candidates are different with K-S probability of 8%.

As shown in Fig. 5, gap sources and BS candidates are the most centrally concentrated populations. There are two possible physical explanations for this: (1) Since CVs and BSs are expected to be more massive than MS and HB stars, the differences in radial distribution could be an indication of mass segregation; i.e., the heavier objects sink towards the cluster core and end up more centrally concentrated than the lighter MS and HB stars (and WDs). (2) Alternatively, since CVs and BSs in GCs can form through two- or three-body interactions that take place preferentially in the denser cluster core, they may be overabundant there because this is their birthplace.

In any case, the enhanced central concentration of the gap sources provides additional evidence that most of these sources are indeed CVs or non-interacting WD/MS binaries (as opposed to chance superpositions, foreground stars, etc.), i.e. they either segregated towards the cluster centre or formed in the dense core region.

The bottom panel of Fig. 5 shows the radial distribution of only HB stars. We compare EHB and BHB stars, and it seems that EHB stars are slightly more concentrated in the inner $5''$, i.e. the cluster core. As a next step, we compare the EHB and BHB stars only in the cluster core (Fig. 6, top panel) and outside the core region (Fig. 6, bottom panel). We found that the two HB populations in the inner $5''$ are different with K-S probabilities of 7.5%, whereas the EHB and BHB populations in the outskirts (i.e. outside the cluster core) of M 15 appear not to be different, with a K-S test probability of 93.2%. This might indicate that EHB stars are indeed more centrally concentrated than BHB stars. One possible explanation could be that EHB stars have a dynamical origin (Fusi Pecci et al. 1993) and could have formed from mergers of WD binary systems (Iben 1990).

4. Variable candidates

4.1. Detection of Variability

For our variability study only relative magnitudes are needed. For this purpose, we performed photometry on the individual drizzled, i.e. geometrically corrected, images, allowing also for a Gaussian recentering of the input coordinates. We only used exposures taken in

SBC/F140LP, since this data set provides the longest time coverage (from 2004 October 14 to December 5). In total 90 exposures were used for this analysis. Eighty of these had exposure times of 300 s, six were exposed for 40 s and four had exposure times of 140 s (see Table 1).

For each star in our input catalog of FUV sources, its mean magnitude and the corresponding standard derivation were calculated from all single magnitudes. Fig. 7 shows a plot of all mean magnitudes versus their corresponding σ_{mean} for all stars. Based on this plot, we selected 53 sources that show a σ_{mean} exceedingly higher than their companions with similar brightness. These initial variable candidates are marked with plus signs in Fig. 7. As a next step, we checked each of our initial variable candidates by eye on all 90 input images. We found that in a few cases, the recentering algorithm actually centred on the nearest neighbour instead of the source in question. This happened especially for our variable candidate 32, which for a few orbits became extremely faint. In these cases, we forced the photometry on the initial input coordinates without recentering. We caution that for accurate photometry a recentering is usually better, as small shifts between the input images might occur (see Sect. 2.1). However, in the case mentioned above, the recentering fails to work and photometry forced on the initial input coordinates is then the only option available, but it should be considered with some care.

A few initial variable candidates were located in the halos of close bright stars. These stars either are only detectable in the combined master image, but are too faint to show up in the single input images (which can have exposure times as low as 40 s), or they might just be false detections in the halos of bright stars. For our further analysis, these questionable candidates are not considered. Most of these doubtful objects have no NUV counterpart (except for source 2388), which again indicates that they are either very blue and faint sources or indeed false detections. Two variable candidates turned out not to be true sources at all but bad pixels and were consequently deleted from our list of FUV sources in Table 2. We checked that there are no further known bad pixels that coincided with suspected sources. The remaining 41 variable candidates are marked with diamonds in Fig. 7 and are discussed in detail in the following. Note that six of our good variable candidates (V1, V2, V3, V4, V6, and V35) are located outside the NUV field of view. V15 and V40 are inside the common field of view but do not have an NUV counterpart within our chosen tolerance radius of 2.5 pixels. Consequently, these eight variable candidates do not appear in the CMD in Fig. 3. Our notation "Vxx" refers to the variable candidates that we discuss in the present paper. We caution that Clement et al. (2001) use the same nomenclature but for different stars.

Note that the UCXB M 15 X-2 does not show a noticeable σ_{mean}. This source has an or-

bital period of 22.5806±0.0002 minutes, and the signal is clearly significant, see Dieball et al. (2005b). However, the semi-amplitude of its modulation is only 0.062 ± 0.004 mag, which is below our selection criterion in the context of this paper. All our variable candidates have $\sigma_{mean} > 0.2$ mag, and M 15 X-2 would not have been detected as a variable based on Fig. 7, in contrast to the LMXB AC 211, which corresponds to our V21. This shows that we detect stars that show strong variability, but we do not claim to be complete and detect "all" variable stars in the core of M 15. For this, a more thorough variability analysis would be needed, which is beyond the scope of the present paper. We marked the position of the UCXB with a star and indicate it with an arrow in Fig. 7.

In order to check for systematic trends in our data, we analyzed the light curves of the 10 brightest, non-variable stars in our sample. A slight trend of somewhat fainter magnitudes towards the end of each orbit is visible in all of them. The resulting periodograms all peak at a period that is consistent with the *HST's* orbital period.

Fig. 8 to Fig. 10 show the mean-subtracted light curves over all observing epochs for all remaining good variable candidates. We computed χ^2 periodograms for all data sets in order to determine periods for all variable candidates. However, even if present, a periodicity can only be determined if the observations sample that period sufficiently well. This is the case for many but not all variables. A sine wave representing the corresponding period is then overplotted on their light curve. The folded light curves are shown in Fig. 11. Tables 4 and 5 give an overview over all variable candidates, their periods, and their classification based on the following discussions.

4.2. RR Lyrae stars with possible counterparts: V2, V3, V4, V8, V9, V14, V27, V28

RR Lyrae stars are radially pulsating giant stars of spectral class A – F that change their brightness with periods of 0.2 to 1.2 days and amplitudes from 0.5 – 2 mag in V (Kholopov et al. 1988)[5]. RR Lyrae are divided into (at least) two subgroups: RRab show asymmetric light curves and pulsate in the fundamental tone. They show periods from 0.3 to 1.2 days and amplitudes from 0.5 to 2 mag in V. RRc show first-overtone pulsations, their light curves are roughly sinusoidal with periods of 0.2 – 0.5 days and their amplitudes are not greater than 0.8 mag in V.

The light curve of our variables V2, V3 and V4 show long-term variability, with periods

[5]The GCVS is also available at: http://www.sai.msu.su/groups/cluster/gcvs/gcvs/

of 0.3674, 0.2768 days, and 0.2995 days, respectively. Periods and amplitudes agree with these variables being RR Lyrae stars. All of these three sources match within 2″ with the known RR Lyrae V144 in Clement et al. (2001), or BSR 1856 in Tuairisg et al. (2003), and constitute possible counterparts to this object. V2's coordinates match within 0.″5 with the known RR Lyrae and are thus the closest positional match, whereas our V3 and V4 both match within 1.″8 with BSR 1856. Tuairisg et al. (2003) derived a period of 0.2990 days for BSR 1856, which agrees very well with the period of our V4. It is likely that V2 and V3 maybe are newly discovered RR Lyrae whereas V4 is the true counterpart to BSR 1857.

The coordinates of V8 match within 0.″9 with V165 in Tuairisg et al. (2003), for which they derived a period of 0.4339 days. We derived a much smaller period of 0.3644 days, which fits our observed light curve better than a period of 0.4339 days. As a further test, we folded the light curve with our period and a period of 0.4339 days, see Fig. 12. As can be seen, the resulting plot with the longer period does not result in a smooth curve. Although the coordinates agree well enough, the different periods suggest that our V8 is probably not the same source as V165 in Tuairisg et al. (2003).

V9 matches within 1.″1 with V128 in Clement et al. (2001). However, our period is 0.3492 days and thus somewhat shorter than the one Tuairisg et al. (2003) derived for this RR Lyrae, namely, 0.4034 days. Folding the observed light curve with our period and folding with the longer period of 0.4034 days (see Fig. 12) both give reasonably smooth curves. Thus, we cannot exclude that the period derived by Tuairisg et al. (2003) might be the correct one for this RR Lyrae.

V14 and the previously known RR Lyrae V137 in Clement et al. (2001) match within 1.″8, but the periods do not agree with each other. We derived a period of 0.2997 days, which is smaller than the 0.3520 day period Tuairisg et al. (2003) derived. The fit to the observed light curve is better with our shorter period than with a 0.3520 day period. Also, the folded light curves suggest that 0.3520 days is not the correct period for this variable star.

V27 shows a long-term variability with a period of 0.3531 days, which agrees very well with the known RR Lyrae V160 in Clement et al. (2001), for which Tuairisg et al. (2003) derived a period of 0.3529 days. The coordinates of V27 and Tuairisg's V160 match within 2″. NUV information is available for V27, and its location in our FUV–NUV CMD is above the ZAMS and close to the ZAHB. This agrees well with the expected location of RR Lyrae stars.

V28 is within 2″ from the known RR Lyrae V135 (Clement et al., 2001). We derived a period of 0.3615 days for this variable star, which agrees very well with the 0.3619 day period obtained by Tuairisg et al. (2003).

4.3. Newly detected RR Lyrae: V12, V16, V17, V19, V23, V29, V32, V34, V35

The coordinates of our RR Lyrae candidates V12, V16, V17, V19, V23, V29, V32, V34 and V35 do not match those of any known RR Lyrae stars within 2″. All of these sources have FUV_{STMAG} = 18.5 – 21.3 mag and brightness variations of about 2 – 4 mag on a timescale of 0.2 – 0.6 days (see Table 4). Except for V35, NUV information is available for all of them, and V12 and V32 are located between the BS and ZAHB sequence in our CMD in Fig. 3, whereas V16, V17, V23, V29, and V34 lie more or less exactly on the ZAHB track. V19 is somewhat fainter and redder than most of the other RR Lyrae candidates and is located above the faint end of the ZAHB. The positions of all these variable sources agree with the expected location of RR Lyrae stars in the FUV–NUV CMD.

All of the above-mentioned variables can be called RR Lyrae with good confidence, as their periods, amplitudes, and location in the CMD agree with what we expect for this type of variable. However, V12 shows a larger scatter in its light curve than the other RR Lyrae, and its location in the CMD is towards fainter FUV magnitudes. We call this variable a suspected RR Lyrae.

The reason why these RR Lyrae were not found in previous studies could be that optical surveys suffer from severe crowding that increases towards the cluster core. Also, the FUV amplitudes for RR Lyrae are more significant than the optical ones, making them easy to detect. However, we point out that our variability census is not complete as we only consider bright variables with large FUV amplitudes. Variables that either are FUV fainter than 22 mag or have smaller amplitudes, see Fig. 7, are not further discussed in the present paper.

4.4. Previously Suspected Dwarf Novae: HCV2005-A (CV 1) and HCV2005-B

DNe are CVs that show multiple outbursts ranging in (optical) brightness from 2 to 5 mag. The outburst intervals are quasi-periodic but can range from days to decades. The duration of an outburst is typically days to weeks. These outbursts are thought to be due to the release of gravitational energy, which results from an instability in the accretion disk.

In addition to the two LMXBs AC 211 and M 15 X-2, Hannikainen et al. (2005) found four faint X-ray sources within the inner 50″ of M 15. Two of these sources are within our field of view, namely, HCV 2005-A and HCV 2005-B (see Table 6).

Hannikainen et al. (2005) suggested that HCV 2005-A is a probable DN. This source is the same as the DN CV 1 in Shara et al. (2004). This object does not appear in our initial

list of FUV sources and was not noticed when we inspected the FUV master image by eye. The reason for this is that it is very faint and so close to the nearest bright star that the two blend into each other and could not be discriminated. As Shara et al. (2004) pointed out, the DN is in quiescence during their FUV observations and too faint to be detected. Shara et al. (2004) used the same data set as we do but could only use a part of the FUV epochs as the remaining observations were not yet available at that time. In fact, CV 1 is in outburst in our fourth observing epoch, and so we were able to identify this DN (see Fig. 13). This source appears to be undetectable in the WFPC2 1994 April data, on which the Van der Marel et al. (2002) catalog is based, whereas the WFPC2 data taken in 1994 October show a bright source (see also Hannikainen et al. 2005).

The second X-ray source HCV 2005-B is a faint NUV = 21.36 mag object that appears only in our NUV images and is too faint to be detected in our FUV data in any epoch (Fig. 14). Hannikainen et al. (2005) suggested that this source is most likely a DN but might also be a quiescent soft X-ray binary. Unfortunately, we cannot shed more light on the true nature of this object.

4.5. Other Cataclysmic Variables: V7, V11, V15, V39, V40, V41

The light curve of our variable V7 shows brightness variations of a few tenths of a magnitude on short timescales of minutes. CVs can show sizeable variability on a wide range of timescales, and the variation we observe here might be the so-called flickering, which is a random, aperiodic variability seen on timescales of seconds to several minutes and typical for CVs (e.g. Bruch 1992). The location of this variable source in the FUV–NUV CMD is close to the WD cooling sequence, which makes this source an excellent CV candidate. V11, V39, and V41 also are very good CV candidates as their light curves show flickering and they are all located in the gap region in our CMD, see Fig. 3.

V15 and V40 show similar small time-scale variations. As no NUV information is available for those two sources, we call these variables suspected CVs.

4.6. Cepheids: V10

Cepheids are radially pulsating, bright variables with periods of $\approx 1 - 135$ days and variability amplitudes from several hundredths to 2 mag in V. The amplitude in B is larger and increases towards the FUV. Traditionally, both Delta Cep and W Vir stars are called Cepheids as it is often impossible to discriminate between them on the basis of the light

curves for periods in the range 3 – 10 days. However, these are distinct groups of entirely different objects in different evolutionary stages. Delta Cep stars, the classical Cepheids, are relatively young objects belonging to the young disk population. They can be found in open clusters and have just evolved into the instability strip of the Hertzsprung-Russell diagram. W Virginis variables, on the other hand, belong to the old disk population and can be found in GCs and at high Galactic latitudes. They show periods of approximately 0.8 – 35 days and amplitudes from 0.3 to 1.2 mag in V. The period-luminosity relations are different for Delta Cep and W Virginis variables. For more details, see Kholopov et al. (1988).

The coordinates of V10 closely match (within $0\farcs2$) with the Cepheid FP V16, and its period of 1.62 days also agrees with this variable source being a Cepheid star. Tuairisg et al. (2003) found a shorter period of only 1.2411 days for this object, but we note that their estimate is close to one of our aliases in our periodogram. The location of V10 in our CMD is above the ZAHB sequence.

4.7. Other possible Cepheid candidates: V1, V13, V18, V30, V31, V36

The most striking feature in the light curve of our variable V1 is that it brightens by ≈ 3 mag in the fifth observing epoch. This might indicate an outburst, as in DNe. On the other hand, V1 might be a variable with a long-term period, possibly 2.6 days, which might suggest that this source is a Cepheid. We do not have additional NUV information, as this star is located outside the NUV field of view. However, the counterpart to V1 in Van der Marel et al. (2002) is a bright source located on the BHB in the optical CMD (Fig. 4). This suggests that this variable is a Cepheid.

V13 is $\approx 1-2$ mag brighter in the fifth and sixth observing epochs compared to the remaining epochs. This again might indicate an outburst as in DNe, or it might indicate a long-term variability of possibly 3.4 days, which is consistent with a Cepheid periodicity. Its location in our FUV–NUV CMD is above the ZAMS and close to the ZAHB. As CV candidates are expected in the region between the ZAMS and the WD cooling sequence, we suggest that V13 is a Cepheid candidate rather than a CV candidate. The same is true for our variable sources V18, V30, V31, and V36. All sources show an increase in brightness of about 2 mag in at least one observing epoch, which might be indicative of a DN outburst. However, periods of 1.4 days for V18, 4.5 days for V36, and 3.8 days for V30 and V31 fit to the corresponding light curves which might suggest that these stars are Cepheids. V18 and V36 are located above the ZAHB in our FUV–NUV CMD, see Fig. 3, whereas V30 and V31 are located above the ZAMS and below the ZAHB, but close to the location of the previously known Cepheid (our V10). The location of all these variables agrees with the

expected location of Cepheids in our CMD.

We caution that our variable classification is a tentative one, based on the derived periods and the photometric quantities of the variables. This is especially difficult for our Cepheid candidates, as the long periods are not evenly or completely covered by our data set. This is reflected in Fig. 11, which shows the folded light curves for all our variables. As can be seen, there are quite large gaps in the folded light curves for our Cepheid candidates, rendering their classification somewhat uncertain. However, except for V31, all our Cepheid candidates have optical counterparts, and these are all located along the BHB in the optical CMD, the expected location for Cepheid variables.

4.8. Low-mass X-ray binaries: V21/AC 211 and M 15 X-2

V21 is the known LMXB 4U 2129+12 or AC 211. It is not only the brightest variable but also the brightest FUV source in our catalog. This source has a period of 17.1 hr (Ilovaisky et al. 1993) and is one of the optically brightest LMXBs known. The light curve of V21/AC 211 is presented in Fig. 9 and seems to indicate an eclipse during the sixth observing epoch. Unfortunately, our own data coverage is not good enough to derive a reliable period for this source.

As mentioned earlier, the second LMXB in this cluster, M 15 X-2, does not show a large σ_{mean} in Fig. 7. We refer the reader to Dieball et al. (2005b) for a thorough discussion of this UCXB. For the sake of completeness, we include M 15 X-2 in Table 5 and mark this source in our CMD in Fig. 3.

4.9. SX Phoenicis: V33

SX Phoenicis stars are pulsating BSs with short periods of less than 0.1 days (Jeon et al. 2001). They are found in the old disk population and in GCs, and show variability amplitudes of up to 0.7 mag in V.

V33 shows large brightness variation of ≈ 3 mag with a period of 1.32 hr. A sine wave with a corresponding period fits the observed light curve well, see Fig. 10. The coordinates for V33 agree within $0\farcs8$ with the known SX Phoenicis star VGG 10041, which is ZK 62 in Kravtsov & Zheleznyak (2003), who derived a period of 1.248 hr for this variable star. The FUV amplitude is much larger than the optical one. The same effect is known for RR Lyrae stars and Cepheids. Large FUV amplitudes are to be expected since the amplitudes of the pulsations increase towards the FUV (Downes et al. 2004; Wheatley et al. 2004).

4.10. Another SX Phoenicis candidate: V22

Our variable V22 shows a 2 mag brightness variation with a period of 1.06 hr. Its location in our CMD, see Fig. 3, is slightly above the ZAMS and BS track. Its characteristics suggest that it might be an SX Phoenicis star.

4.11. Other suspected variables: V5, V6, V20, V24, V25, V26, V37, V38

The light curve of V5 shows a small-amplitude scatter, but the most striking feature is the rise in brightness at the end of the first observing epoch, which might correspond to an egress from an eclipse, or the beginning of an outburst as in DNe. The source is faint in the second, third, fourth, and sixth observing epochs, but brighter in the fifth observing epoch, which fits the characteristics of a DN. The source is located between the BS and ZAHB sequence in our FUV–NUV CMD, see Fig. 3. However, its optical counterpart is located on the BHB in the optical CMD. If this source is indeed a DN in M15, its optical counterpart is unusually bright. Further observations are required to shed more light on this variable source.

The light curve of V6 shows a considerable drop in brightness in the second, third, and fifth observing epochs. The characteristics of the light curve match that of a DN. In this case, V6 seems to be in outburst during the first, fourth, and sixth observing epochs. This would imply an unusually high duty cycle of 70% of the time coverage. Unfortunately, this star is located outside the NUV field of view. However, we do have an optical counterpart to this source, which is a rather unexpected one: it is one of the brightest optical sources, and its location in the optical CMD is blueward of the tip of the RG branch at $V = 12.953$ and $B - V = 0.737$ mag (see Fig. 4). Its optical magnitude is far too bright to agree with a DN at the distance of M 15. A possible explanation is that the optical counterpart is a "mismatch" (although the FUV and optical coordinates agree within $0\farcs0165$), and the "true" optical source might be an undetected, faint source in nearly the same line of sight as the bright one. Another, and perhaps more likely, explanation is that this source is a variable field star that happens to be in our line of sight. If it is a field DN, it would be much closer to us than M 15, i.e. at least 400 pc assuming an absolute $M_V = 5$ mag for a DN in outburst.

Our variable V20 shows flickering and in addition reveals some long-term variability. It is brightest during our first, third, fourth, and fifth observing epochs. This might indicate outburst activity, as in DNe. It is also possible that V20 is a CV of VY Scl type, which show sudden drops in brightness. If this is true, V20 might be in a low state in the second and sixth observing epochs. On the other hand, its light curve could also be explained with

a Cepheid-type long-term periodicity of 1.5 days. This suspected variable is a bright source and is located just below the ZAHB in our CMD. Based on its light curve and location in the CMD alone, we cannot decide whether this source might be a bright CV or a bright Cepheid, and further observations are required to decide on the nature of this variable.

V24 is located above the clump of MS stars and RGs and on the lower (fainter) part of the ZAHB in our FUV–NUV CMD. From its location in the FUV–NUV CMD, it might well be an FUV fainter but redder BS or a BHB star. However, the optical counterpart to this source is located on the BHB in the optical CMD. This suggests that this source might be a binary or pulsating HB star.

The light curve of V25 shows some small-scale brightness variation on short time-scales, possibly flickering. However, in addition to the flickering, a long-term variability seems to be superposed, which can be seen in the first observing epoch where the source is ≈ 2 mag fainter towards its end. The location of V25 in our CMD is on the lower, fainter part of the ZAHB. This source is difficult to classify, and it might be a binary or pulsating BS or HB star.

V26, V37, and V38 show flickering with a few tenths of a magnitude variation on short time-scales. Their location in the FUV–NUV CMD is close to the ZAMS and they might be either bright CVs or binary or pulsating BSs. Only V37 has an optical counterpart, but its optical magnitudes agree again with a BS or a bright CV.

4.12. Variability Census and its Implications

We found 41 sources that show strong signs of variability. Based on the appearance of their light curve (Figs. 8 to 10), their period, and their location in the FUV–NUV and in the optical CMDs (Figs. 3 and 4), we suggest classifications for our variable sources. We compared the coordinates and periods, if available, of our variable sources with known variables in the core region of M 15. In total, we found 17 RR Lyrae stars (4 of which are known), 6 CV candidates, 1 known SX Phoenicis star, 1 SX Phoenicis candidate, 1 previously known Cepheid and 6 further candidates, and the known LMXB AC 211. The 8 remaining suspected variables cannot be classified clearly, but most of them might be CVs or pulsating/binary BSs.

Note that only six out of our gap objects show strong signs of variability. However, the remaining gap objects might also be variable, but they are either fainter or have smaller amplitudes and thus were not detected in our variability study, see Fig. 7. (We note again that, for example, the UCXB M 15 X-2 was not detected as a strongly variable source in

this study, as it shows a modulation with only 0.062 mag semi-amplitude; see Dieball et al. 2005b.) We marked the gap objects that we selected based on our FUV–NUV CMD as red filled circles in Fig. 7. The green filled circles denote the two sources that do not have an NUV counterpart, and thus do not appear in our FUV–NUV CMD, but are likely CVs because of their variability. There are ≈ 60 gap objects/CV candidates. Typical short-timescale variability for a CV is flickering with amplitudes of a few tenths of a magnitude. As can be seen from Fig. 7, there are 25 gap sources that show a $\sigma_{mean} > 0.5$ mag, but most of these are located in the bulge of faint sources at $\mathrm{FUV}_{mean} > 22$ mag and thus were not considered in the above study. We consider these sources good CV candidates. This number agrees with our previous estimate, see Sect. 3.4.

5. Summary

We have analyzed deep FUV *HST* ACS observations of the core of the metal-poor GC M 15. Based on our FUV and NUV data, we constructed a CMD in which various stellar populations are present. Our CMD is deep enough that MS stars and RGs show up. The MS turnoff is visible at FUV $\simeq 23.5$ mag and FUV–NUV $\simeq 3$ mag, and the MS stars and RGs form a prominent data clump that extends at least 2 mag below the MS turnoff. As such, this is the deepest FUV CMD presented so far. A line of ≈ 70 BS candidates and a well-defined sequence of ≈ 130 HB stars are present in our CMD. BHB stars are located along the well-defined HB sequence, whereas EHB stars are clustered within a bright data clump. Approximately 30 WD candidates are found close to the WD cooling sequence, which is well within the expected number of WDs in our field of view down to FUV $\simeq 22.5$ mag. The region between the WD cooling sequence and the ZAMS and BS track is occupied by ≈ 60 objects. Theoretical considerations suggest that at least some of these are CVs. We caution that these numbers should not be taken as exact, since the discrimination between the various zones in our CMD is difficult. The cumulative radial distributions of the stellar populations in our FUV–NUV CMD suggest that gap sources and BS candidates are the most centrally concentrated populations. This might be the expected effect of mass segregation; i.e., more massive stars and binaries like CVs and BSs sink towards the cluster core. Alternatively, it might reflect the preferred birthplace of such objects, as CVs and BSs are thought to be dynamically formed and as such are preferentially found in the dense cluster core. We found that also EHB stars are more concentrated in the core region than BHB stars. This might indicate that at least some EHB stars also have a dynamical origin.

We searched for variability among our FUV catalog stars and found 41 variable sources. They are distributed over the entire CMD, but most of them are located around either the

ZAHB or the ZAMS. Periods could be derived for 27 variables. Based on their variability properties and their location in the FUV–NUV CMD, we suggest classifications for 33 variables. Seven variable sources could be identified with previously known variables.

In total, we found four known RR Lyrae stars, 13 additional RR Lyrae candidates, six CV candidates, two SX Phoenicis stars (of which one is known), seven Cepheids (one previously known), and the known LMXB AC 211. The eight remaining suspected variables cannot be classified clearly, but most of them might be CVs or pulsating/binary BSs. We found that the brightness variations for RR Lyrae stars, Cepheids, and SX Phoenicis stars are a few magnitudes in the FUV and thus much larger than in the optical. This is to be expected since the amplitudes of the pulsations increase towards the FUV (Downes et al. 2004; Wheatley et al. 2004). However, this is the first time such large-scale FUV amplitudes have been observed for SX Phoenicis stars. Note that out of our 60 gap objects/CV candidates, only 6 show strong signs of variability. However, 25 of the gap sources show $\sigma_{mean} \geq 0.5$ mag. We consider at least these to be good CV candidates. This number agrees with theoretical predictions.

All previously known X-ray sources and DNe that are located in our field of view are detected in our UV study. The LMXB AC 211 is the brightest FUV source in our sample, and also the UCXB M 15 X-2 is among the brightest sources. HCV 2005-A and HCV 2005-B (Hannikainen et al. 2005) are both detected in our NUV data set, although HCV 2005-B appears only as a faint NUV source and is not detected in the FUV. HCV 2005-A or CV 1 (Shara et al. 2004) is in outburst in our fourth FUV observing epoch, but otherwise it is too faint to be detected in the FUV.

Overall, the results of our study confirm that FUV observations are particularly well suited in studying hot, and especially dynamically-formed, stellar populations like CVs, BSs, and X-ray binaries in the cores of GCs. They are also a powerful tool in detecting new variable stars in the dense core regions of GCs where optical studies are hampered by the immense crowding. In addition, the large FUV amplitudes of especially RR Lyrae stars, Cepheids, and SX Phoenicis stars make them easily detectable as variables in this wave band.

All clusters that have been studied so far in the FUV, namely, 47 Tuc, NGC 2808, and M 15, revealed large numbers of gap objects that were more or less consistent with theoretical predictions for dynamically formed CVs. It is interesting to directly compare NGC 2808 and M 15, as both clusters now have been studied in both the FUV and NUV, with a full coverage of the cluster cores. Table 7 lists the cluster parameters taken from Harris (1996) and the number of gap objects and BS and WD candidates found in the clusters. As can be seen, slightly more gap sources were detected in NGC 2808 than in M 15, whereas more BS candidates are present in M 15 than in NGC 2808. Evidence for a concentration of the

more massive CVs and BSs is more evident in NGC 2808 (see Dieball et al. 2005a, their Fig. 4), which is somewhat contrary to the longer relaxation time for the cluster's core (see Table 7). However, we caution that these are still small number statistics, so their difference is not particularly significant. We are currently working on data of more clusters. Our current sample with just two GCs is too small to draw any conclusions about the impact of a difference in the binary populations on the cluster evolution. However, the large number of exotica and massive binaries found in the cores of these clusters agrees with theoretical expectations for evolved clusters.

We are grateful to an anonymous referee for a valuable discussion that helped us to improve this paper. DH acknowledges the Academy of Finland. This work was supported by NASA through grant GO-9792 from the Space Telescope Science Institute, which is operated by AURA, Inc., under NASA contract NAS5-26555.

REFERENCES

Arellano, F. A., Garca, L. G. & Rosenzweig, P. 2006, RMxAA, 42, 75

Aurière, M., Le Fèvre, O. & Terzan, A. 1984, A&A, 138, 415

Baumgardt, H., Hut, P., Makino, J., McMillan, S. & Portegies Zwart, S. 2003, ApJ, 582, L21

Brown, T. M., Sweigart, A. V., Wayne B. L. & Hubeny, I. 2001, ApJ, 562, 368

Bruch, A. 1992, A&A, 266, 237

Charles, P. A., Clarkson, W. I. & van Zyl, L. 2002, New Astronomy, 7, 21

Clement, C., Muzzin, A., Dufton, Q. et al. 2001, AJ, 122, 2587

D'Antona, F., Vietri, M. & Pesce, E. 1995, MNRAS, 272, 730

De Marchi, G. & Paresce, F. 1994, ApJ, 422, 597

De Marchi, G. & Paresce, F. 1996, ApJ, 467, 658

Dieball, A., Knigge, C., Zurek, D., Shara, M.M. & Knox, L. 2005a, ApJ, 625, 156

Dieball, A., Knigge, C., Zurek, D., Shara, M.M. & Knox, L. 2005b, ApJL, 634, L105

Di Stefano, R. & Rappaport, S. 1994, ApJ, 423, 274

Dorman, B. 1992, ApJS, 81, 221

Dotani, T., Inoue, H., Murakami, T., Nagase, F. & Tanaka, Y. 1990, Nature, 347, 534

Downes, R. A., Margon, B., Homer, L. & Anderson, S. F. 2004, AJ, 128, 2288

Edmonds, P. D., Gilliland, R. L., Heinke, C. O. & Grindlay, J. E. 2003a, ApJ, 596, 1177

Edmonds, P. D., Gilliland, R. L., Heinke, C. O. & Grindlay, J. E. 2003b, ApJ, 596, 1197

Elson R, Hut P. & Inagaki S. 1987, ARA&A, 25, 565

Fusi Pecci, F., Ferraro, F. R., Bellazzini, M. et al. 1993, AJ, 105, 1145

änsicke, B. T., Beuermann, K. & de Martino, D. 1995, A&A, 303, 127

Gebhardt, K., Pryor, C., Williams, T. B., Hesser, J. E. & Stetson, P. B. 1997, AJ, 113, 1026

Gerssen, J., Van der Marel, R. P., Gebhardt, K. et al. 2002, AJ, 124, 3270

Grindlay, J. E., Heinke, C., Edmonds, P. D. & Murray, S. S. 2001, Science, 292, 2290

Guhathakurta, P., Yanny, B., Schneider, D. P. & Bahcall, J. N. 1996, AJ, 111, 267

Hannikainen, D. C., Charles, P. A., van Zyl, L. et al. 2005, MNRAS, 357, 325

Harris, W.E. 1996, Astronomical Journal, 112, 1487

Heinke, C. O., Grindlay, J. E., Edmonds, P. D. et al. 2005, ApJ, 625, 796

Heinke, C. O., Grindlay, J. E., Lugger, P. M. et al. 2003, ApJ, 598, 501

Hut, P., McMillan, S., Goodman, J., Mateo, M., Phinney, E. S. et al. 1992, PASP, 104, 981

Iben, I. J. 1990, ApJ, 353, 215

Ilovaisky, S. A., Aurière, M., Kock-Miramond, L. et al. 1993, A&A, 270, 139

Ivanova, N., Heinke, C. O., Rasio, F. A. et al. 2006, MNRAS, 372, 1043

Jeon, Y.-B., Kim, S.-L., Lee, H. & Lee, M. G. 2001, AJ, 121, 2769

Kholopov, P.N., Samus, N.N., Frolov, M.S., Goranskij, V.P., Gorynya, N.A. et al. 1988, General Catalog of Variable Stars (4th ed.; Moscow: Nauka)

Knigge, C., Zurek, D. R., Shara, M. M. & Long, K. S. 2002, ApJ, 579, 752

Knigge, C., Zurek, D. R., Shara, M. M., Long, K. S. & Gilliland, R. L. 2003, ApJ, 599, 1320

Kravtsov, V. V. & Zheleznyak, A. P. 2003, Information Bulletin on Variable Stars, 5452, 1

Kulkarni, S. R., Goss, W. M., Wolszczan, A. & Middleditch, J. 1990, ApJ, 363, L5

McNamara, B. J., Harrison, T. E. & Anderson, J. 2003, ApJ, 595, 187

McNamara, B. J., Harrison, T. E. & Baumgardt, H. 2004, ApJ, 602, 264

Oosterhoff, P. T. 1939, The Observatory, 62, 104

Peterson, R. C., Seitzer, P. & Cudworth, K. M. 1989, ApJ, 347, 251

Phinney, F. S. 1996, The origins, evolution, and destinies of binary stars in clusters, Astronomical Society of the Pacific Conference Series, Volume 90, p. 163

Richer, H. B., Fahlman, G. G., Ibata, R. A. et al. 1997, ApJ, 484, 741

Shara, M. M., Hinkley, S., Zurek, D. R., Knigge, C. & Bond, H. E. 2004, AJ, 128, 2847

Shara, M. M. & Hurley, J. R. 2006, ApJ, 646, 464

Silbermann, N. A. & Smith, H. A. 1995, AJ, 110, 704

Sirianni, M., Jee, M.J., Bentez, N. et al. 2005, PASP, 117, 1049

Smale, A. P. 2001, ApJ, 562, 957

Stetson, P. B. 1991, in 3rd ESO/ST-ECF Garching - Data Analysis Workshop, eds. Grosbøl P. J., Warmels R. H., p. 187

Tout, C. A., Pols, O. R., Eggleton, P. P. K., de Martino, D. & Han, Z. 1996, MNRAS, 281, 257

Townsley, D. M. & Bildsten, L. 2003, ApJ, 596, L227

Tuairisg, S. O., Butler, R. F., Shearer, A. et al. 2003, MNRAS, 345, 960

van den Bosch, R., de Zeeuw, T., Gebhardt, K., Noyola, E. & van de Ven, G. 2006, ApJ, 641, 852

Van der Marel, R. P., Gerssen, J., Guhathakurta, P., Peterson, R. C. & Gebhardt, K. 2002, AJ, 124, 3255

Wheatley, J. M., Welsh, B. Y., Siegmund, O. H. W. et al. 2004, ApJ, 619, L123

White, N. E. & Angelini, L. 2001, ApJ, 561, L101

Wood, M. A. 1995, Lecture Notes in Physics, 443, 41

Yanny, B., Guhathakurta, P., Bahcall, J. N. & Schneider, D. P. 1994, AJ, 107, 1745

Table 3: Encircled energy fractions and sky corrections for apertures of 1 to 10 pixels. The encircled energy fractions for the SBC/F140LP data were determined using curves of growth for isolated stars in the SBC/F140LP master image; the encircled energy fractions for the HRC/F220W were taken from Sirianni et al. (2005).

aperture		encircled energy fraction		sky correction	
[pixels]	[″]	HRC/F220W	SBC/F140LP	HRC/F220W	SBC/F140LP
1	0.025	0.235	0.10	1.014	1.02
2	0.050	0.506	0.29	1.014	1.03
3	0.075	0.623	0.45	1.025	1.04
4	0.100	0.686	0.54	1.039	1.06
5	0.125	0.733	0.60	1.057	1.09
6	0.150	0.758	0.64	1.081	1.13
7	0.175	0.771	0.66	1.110	1.17
8	0.200	0.782	0.68	1.145	1.23
9	0.225	0.791	0.70	1.186	1.29
10	0.250	0.801	0.72	1.235	1.37

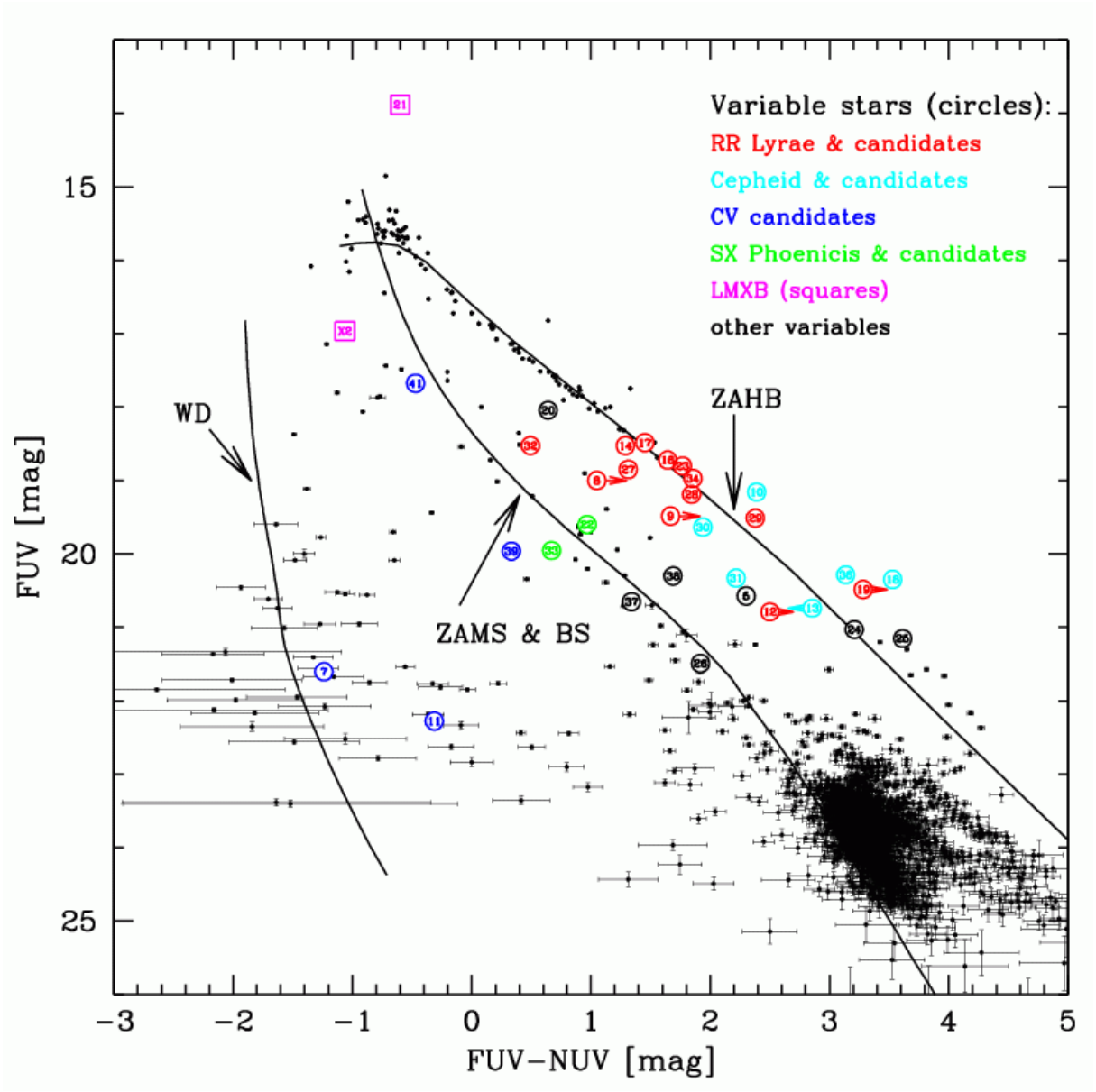

Fig. 3.— FUV–NUV CMD of the core region of M 15. For orientation purposes, we include a theoretical WD cooling sequence, a ZAMS, and a ZAHB (see text for details). The circles and the corresponding numbers denote variable FUV sources, as discussed in Sect. 4. The location of the UCXB M 15 X-2 is also indicated with a magenta square. The brightest FUV star detected, V21, corresponds to the luminous LMXB AC 211, see Sect. 4.8.

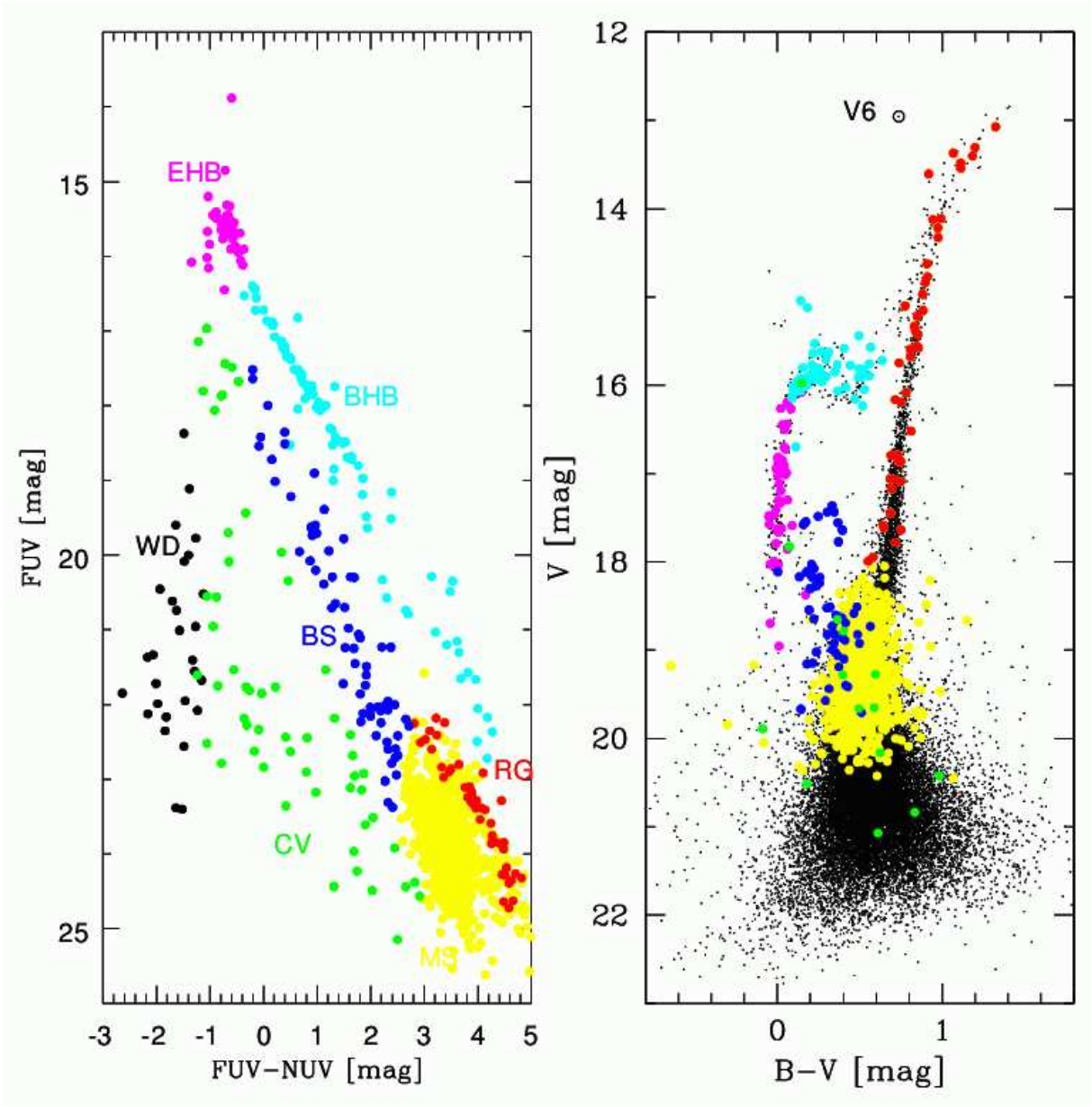

Fig. 4.— Comparison between the various stellar populations found in our FUV–NUV CMD (left) and the optical CMD (right; based on the Van der Marel et al. (2002) catalog). The stellar populations are at their expected location in the optical CMD; i.e., our BS candidates are mainly above the MS turnoff in the optical CMD, etc. (see text for details). Gap objects (which include CV candidates) are plotted in green, BS candidates in blue, MS stars in yellow, RGs in red, EHB stars in magenta and BHB stars in cyan. Note that we did not find any optical counterparts to our WD candidates. The counterpart to our variable candidate V6 is indicated in the optical CMD (right).

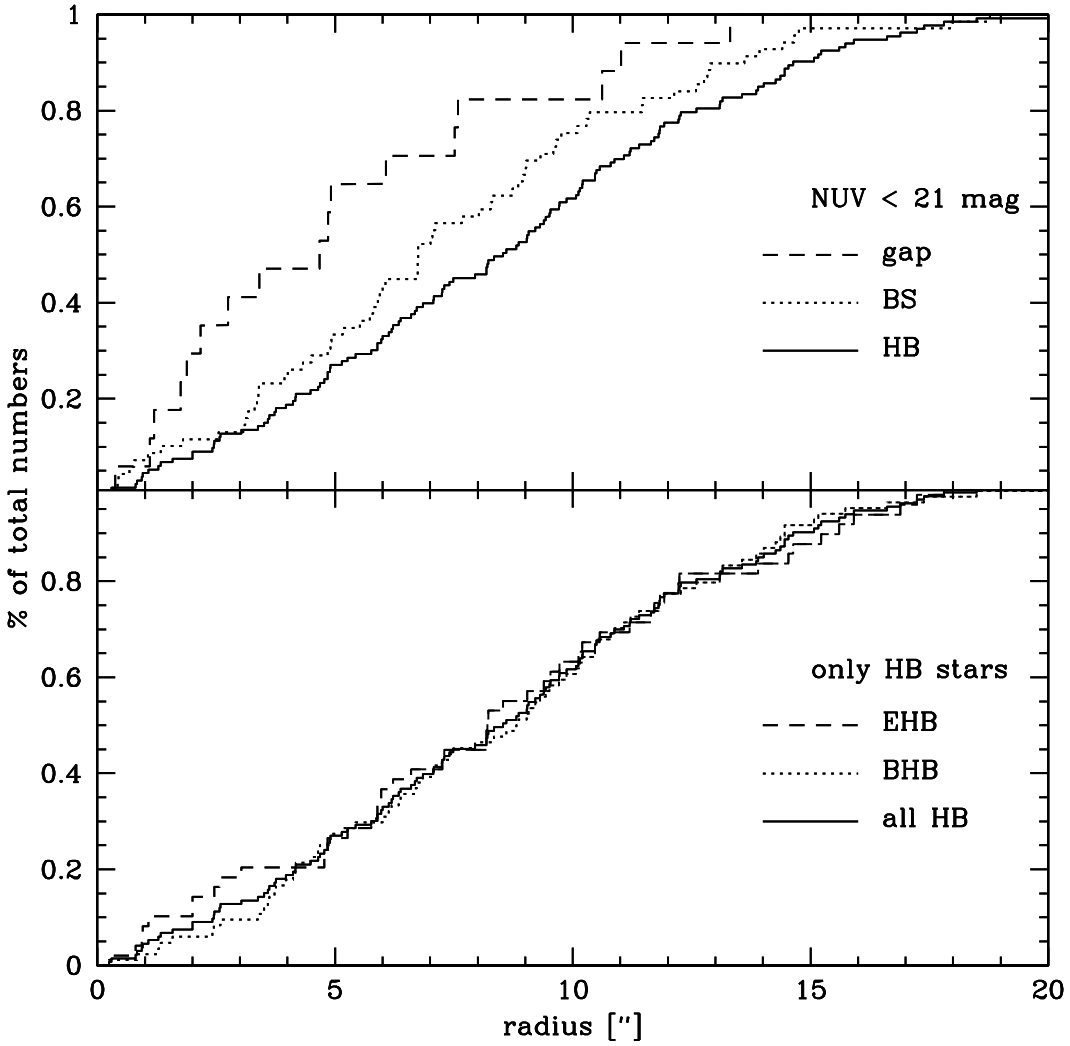

Fig. 5.— Cumulative radial distributions of the various stellar populations that show up in our FUV–NUV CMD. Top: Only sources with NUV $\leq$ 21 mag are considered. We only compare BS candidates (dotted line), gap objects (dashed line), and HB stars (solid line), as only two WD candidates are present that are brighter than 21 mag in the NUV. Bottom: Radial distribution of BHB stars (dotted line) and EHB stars (dashed line). EHB stars seem to be slightly more concentrated in the core. See text for details.

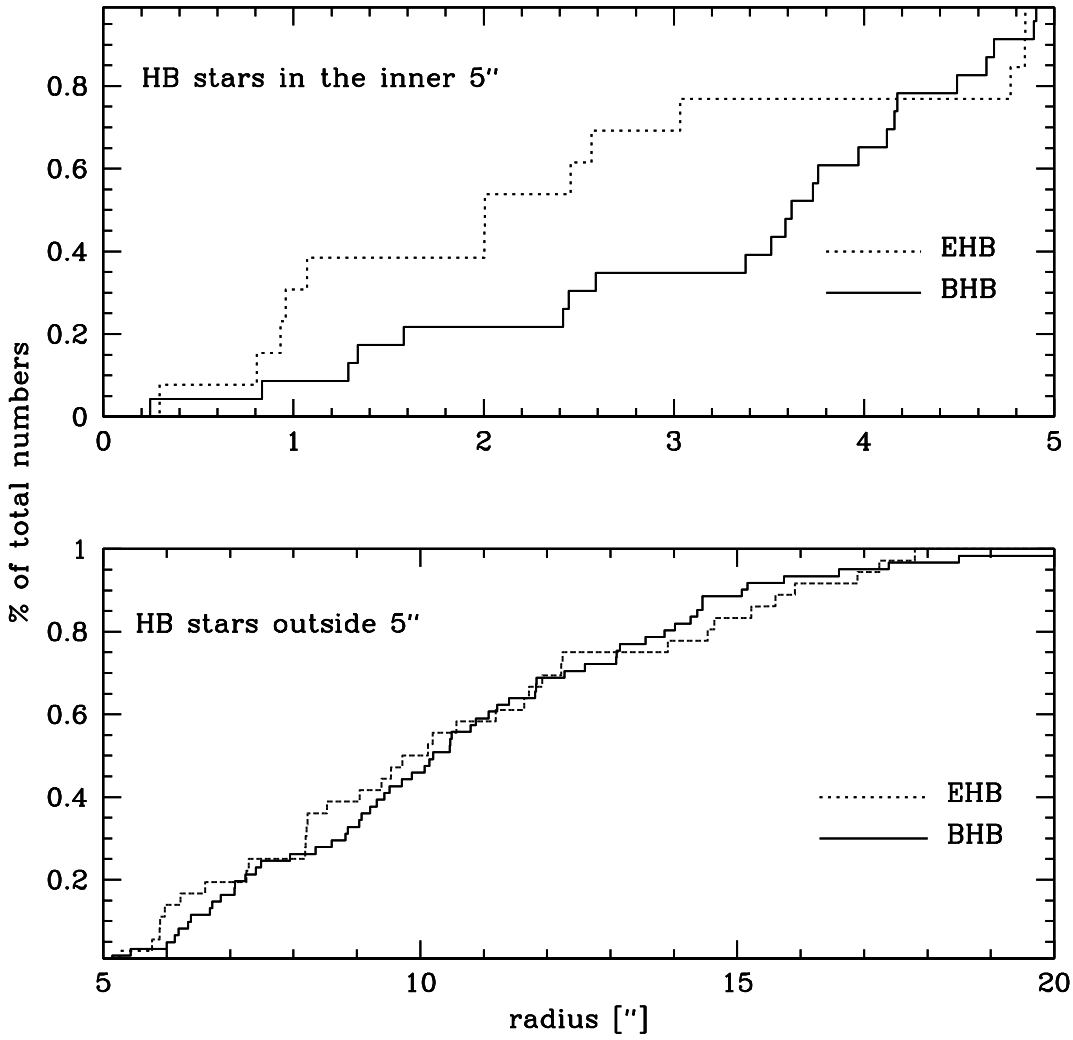

Fig. 6.— Cumulative radial distributions of EHB and BHB stars in the inner 5″ (top) and outside the core region (bottom).

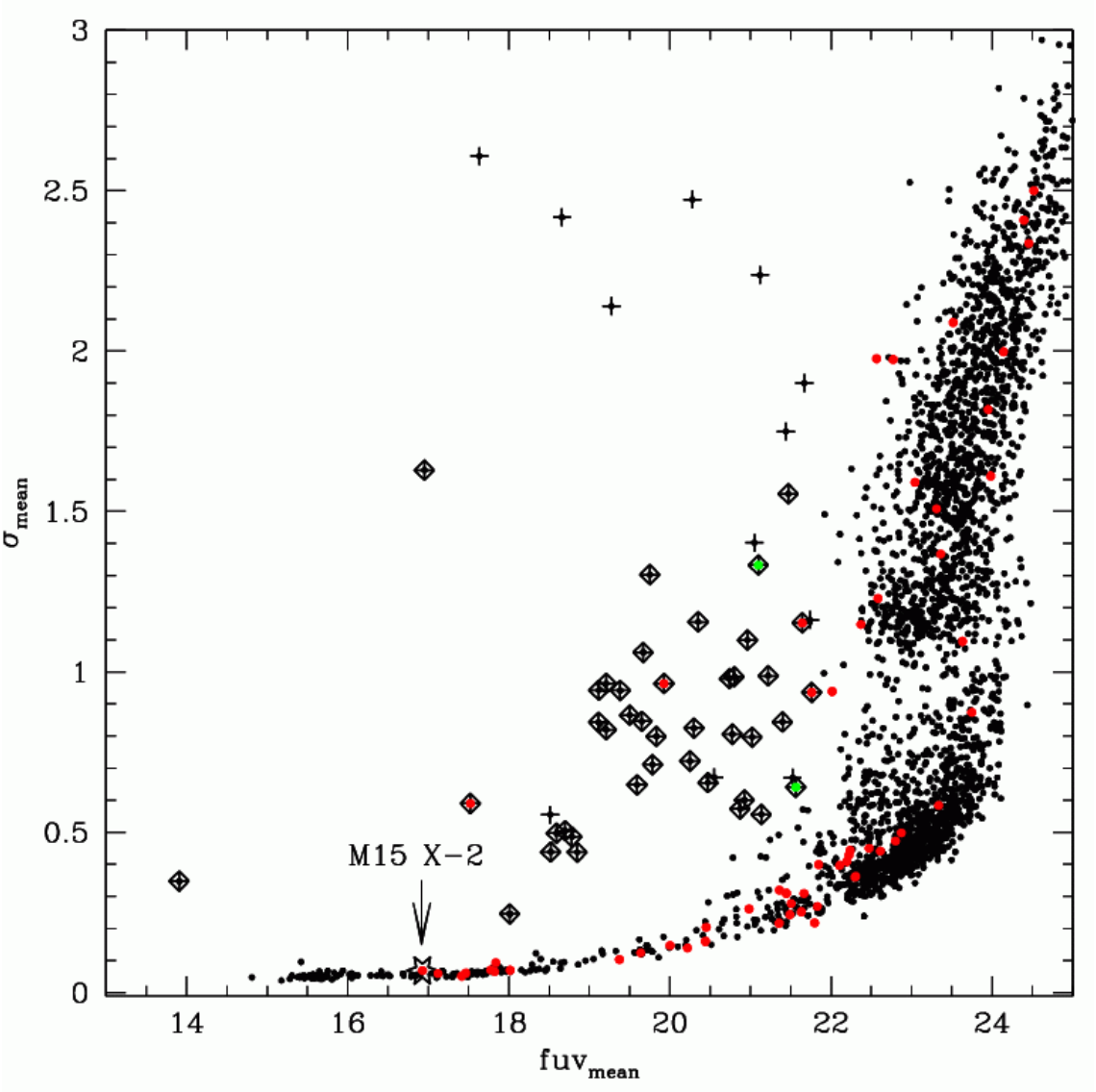

Fig. 7.— Mean FUV magnitudes vs. σ_{mean} derived from the individual photometry of each star. The 53 initial variable candidates are marked with plus signs. The 41 variable candidates that remain after closer inspection on the individual input images are additionally marked with diamonds. The position of M 15 X-2 is marked with a star and indicated with an arrow. The gap objects/CV candidates that we selected based on our FUV–NUV CMD are marked with red filled circles. The two additional objects (V15 and V40) that do not have an NUV counterpart but are likely CVs because of their variability are marked with green filled circles. See text for details.

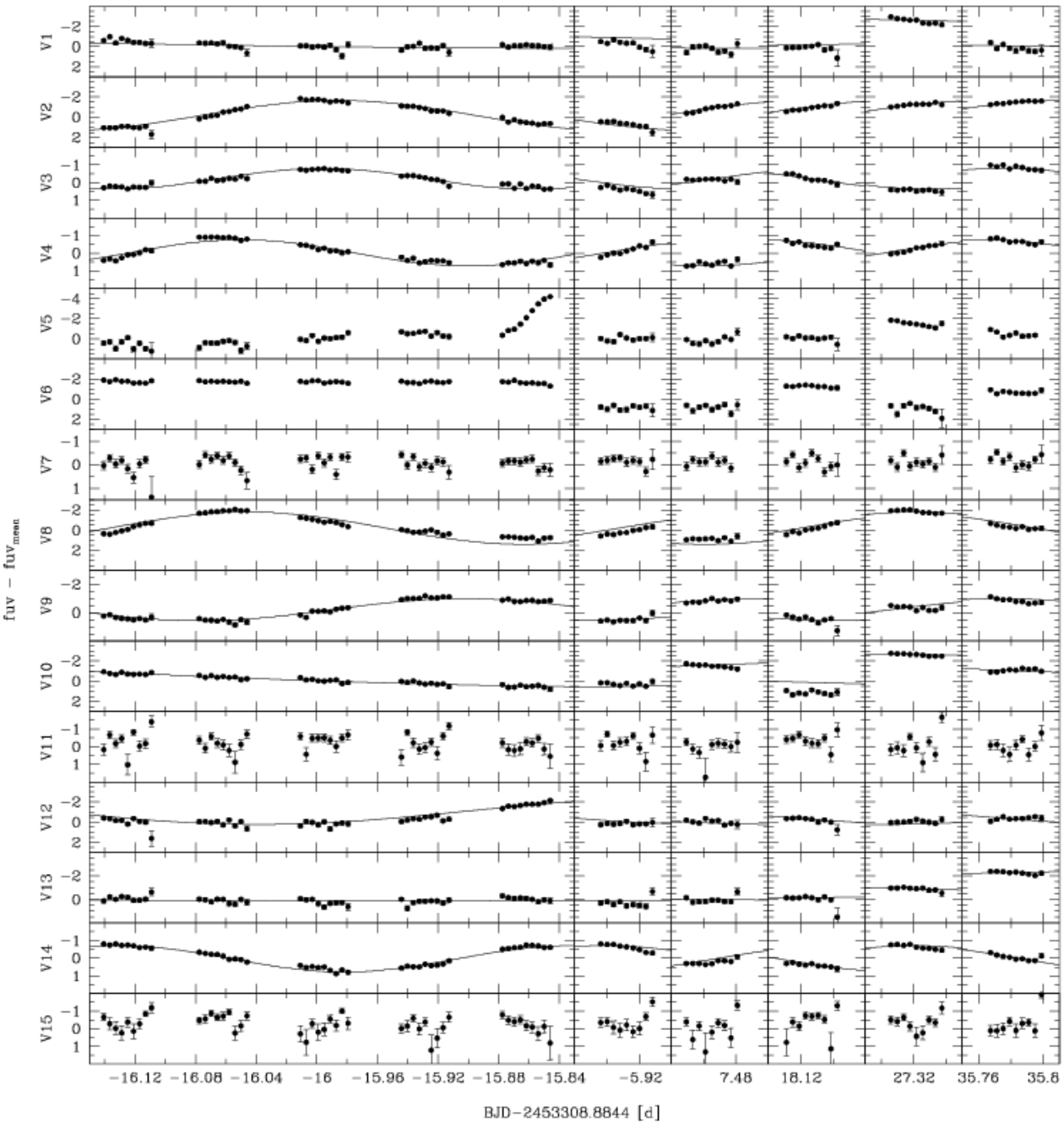

Fig. 8.— Light curves for our variable sources V1 – V15. The mean subtracted instrumental magnitudes are plotted vs. time.

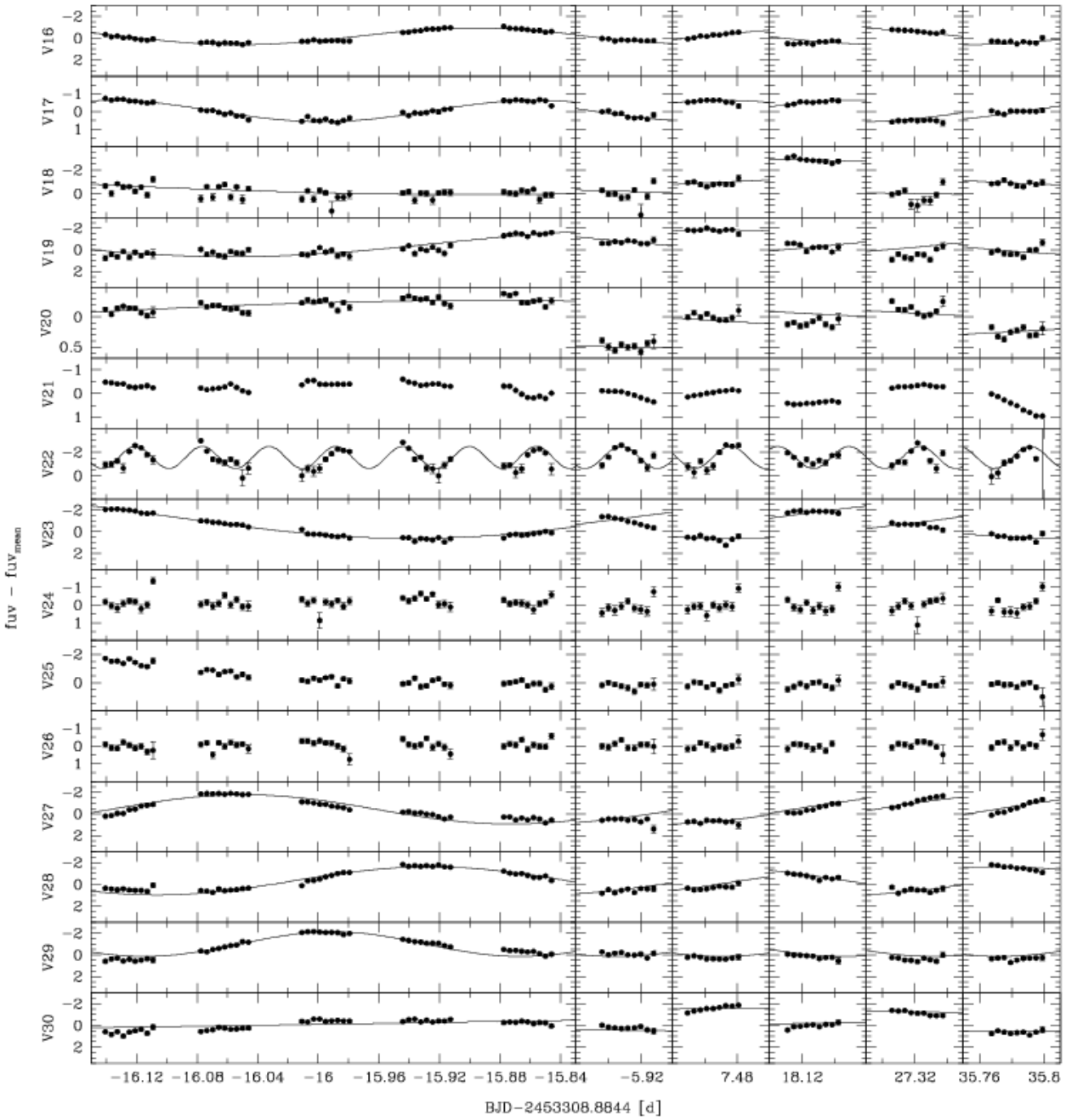

Fig. 9.— Same as Fig. 8, but for the variable sources V16 – V30.

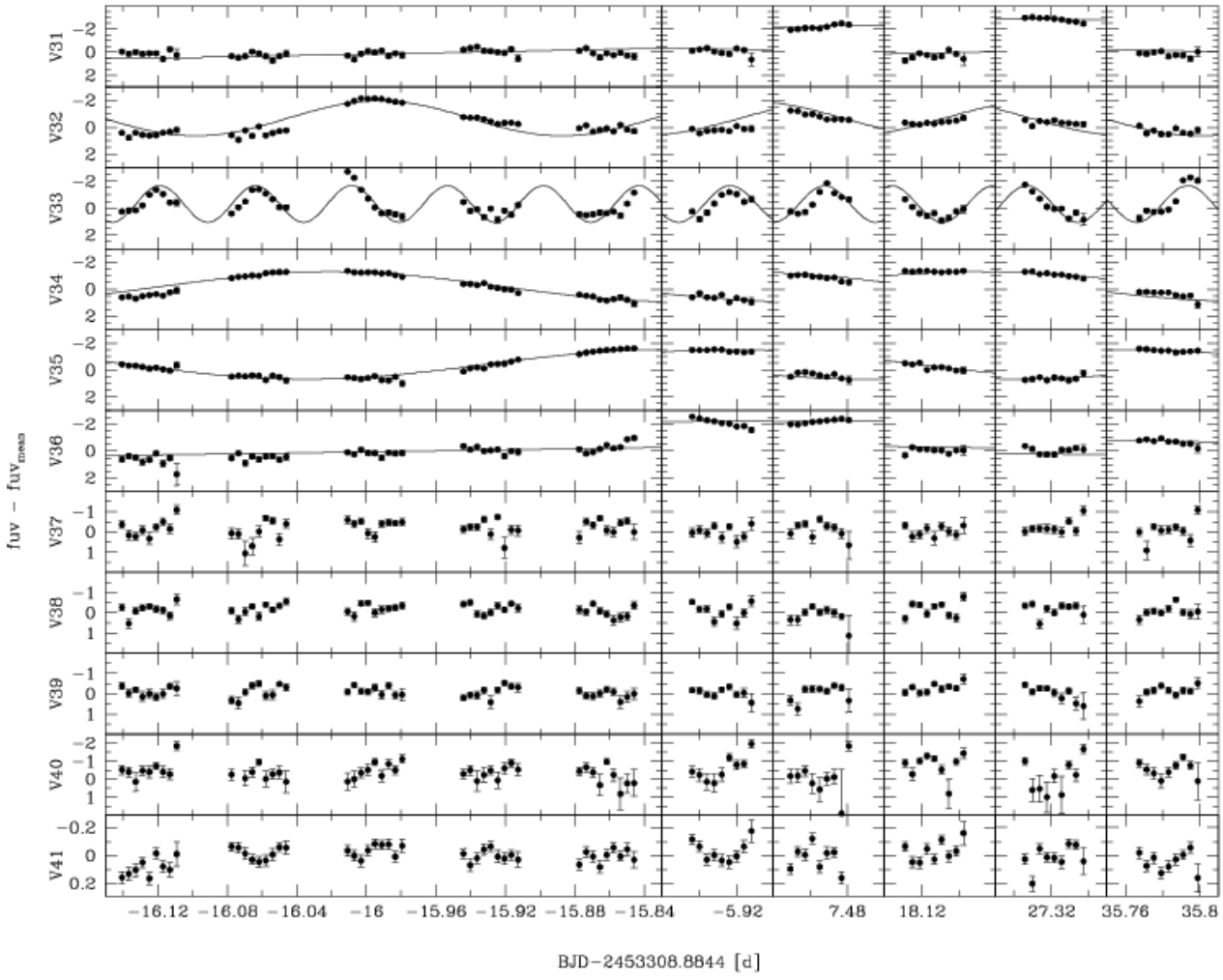

Fig. 10.— Same as Fig. 8, but for the variable sources V31 – V41.

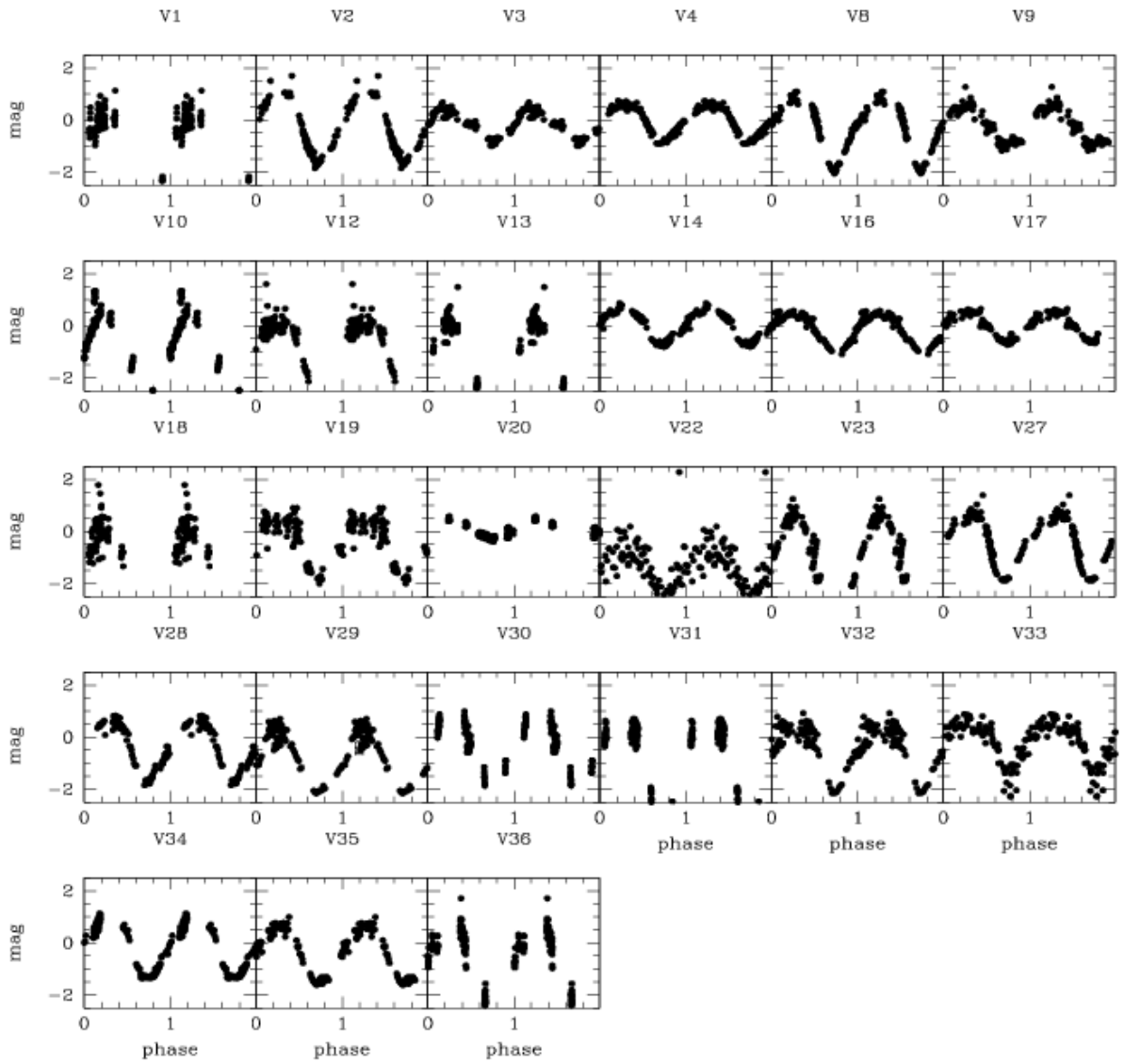

Fig. 11.— Folded light curves for the variables for which we derived periods. See also Table 4 and 5.

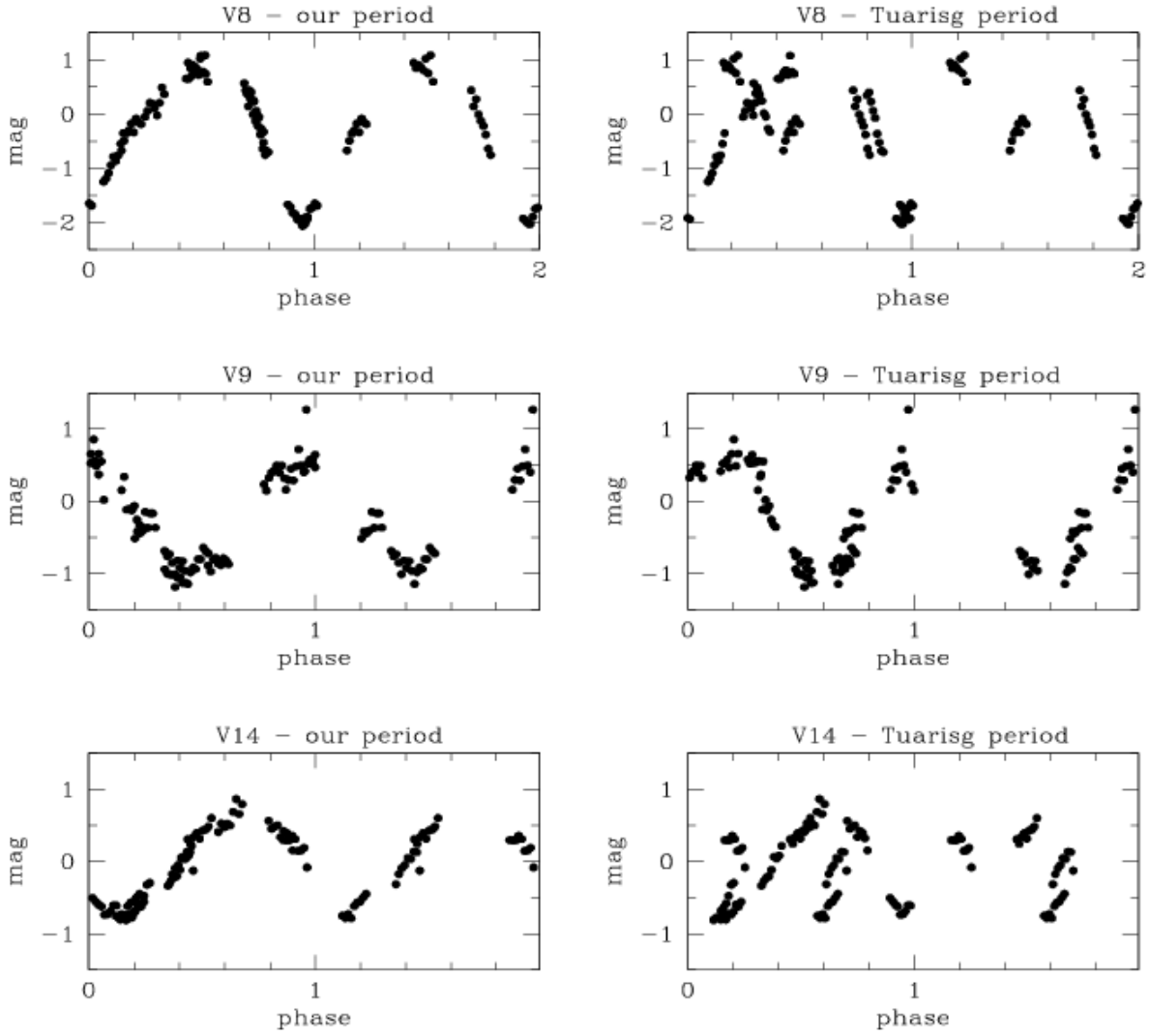

Fig. 12.— Folded light curves for the RR Lyrae V8, V9, and V14. The left panels shows the light curves folded with the periods derived in this paper, while the right panels shows the light curves folded with a period derived by Tuairisg et al. (2003). See text for details.

Table 4: Known RR Lyrae stars and RR Lyrae candidates. Reference for the known RR Lyrae is Tuairisg et al. (2003).

id	$< FUV >$ [mag]	$< FUV - NUV >$ [mag]	period [d]	other name
V2	18.845	–	0.3674	BSR 1856, V144?
V3	18.795	–	0.2768	BSR 1856, V144?
V4	18.619	–	0.2995	BSR 1856, V144 (most likely counterpart)
V8	18.999	1.300	0.3644	V165?
V9	19.485	1.917	0.3492	V128
V12	20.790	2.700	0.5350	
V14	18.526	1.290	0.2997	V137?
V16	18.722	1.643	0.3083	
V17	18.485	1.452	0.2811	
V19	20.485	3.483	0.5408	
V23	18.801	1.768	0.6161	
V27	18.849	1.314	0.3531	V160
V28	19.189	1.845	0.3615	V135
V29	19.512	2.379	0.2483	
V32	18.525	0.493	0.2110	
V34	18.972	1.854	0.3973	
V35	19.398	–	0.4127	

Fig. 13.— Close-up of the DN CV 1 or HCV 2005-A that was in outburst only in our fourth FUV observing epoch (left) but was in quiescence during all other FUV observing periods (middle). The right panel shows a close-up in the NUV. Note that we used the same orientation for these finding charts as Hannikainen et al. (2005) and Charles et al. (2002); i.e., north is to the upper left corner and east to the lower left. CV 1 is marked with a circle and is located at $\alpha = 21^h29^m58.275^s$, $\delta = 12°10'00''.1$. The field of view of these close-ups is $\approx 1'' \times 0''.7$.

Table 5: Classification of all other variables. Periods are in days unless otherwise stated. References for the known variables are: (a) Tuairisg et al. (2003), (b) Ilovaisky et al. (1993), (c) Kravtsov & Zheleznyak (2003), (d) Dieball et al. (2005b).

id	$< FUV >$ [mag]	$< FUV - NUV >$ [mag]	period [d]	type	other name
V1	20.967	–	2.6	CEP candidate	
V5	20.573	2.301	–	?	
V6	19.985	–	–	?	
V7	21.604	-1.238	–	CV candidate	
V10	19.157	2.389	1.6	CEP	V16 (a)
V11	22.277	-0.313	–	CV candidate	
V13	20.739	2.656	3.4	CEP candidate	
V15	21.364	–	–	CV candidate	
V18	20.347	3.530	1.4	CEP candidate	
V20	18.043	0.641	1.5	? (BHB zone)	
V21	13.881	-0.598	17.1 [hrs] (b)	LMXB	AC211 (b)
V22	19.599	0.968	1.06 [hrs]	SXPHE candidate	
V24	21.030	3.209	–	? (BHB zone)	
V25	21.153	3.613	–	? (BHB zone)	
V26	21.492	1.919	–	? (BS zone)	
V30	19.635	1.938	3.8	CEP candidate	
V31	20.328	2.218	3.8	CEP candidate	
V33	19.954	0.670	1.32 [hrs]	SXPHE	VGG 10041 (c)
V36	20.285	3.137	4.5	CEP candidate	
V37	20.651	1.342	–	? (BS zone)	
V38	20.300	1.689	–	? (BS zone)	
V39	19.962	0.333	–	CV candidate	
V40	21.692	–	–	CV candidate	
V41	17.676	-0.469	–	CV candidate	
–	16.964	-1.062	22.6 [min] (d)	UCXB	M 15 X-2 (d)

Table 6: Cartesian coordinates in the NUV master image and NUV magnitudes for the two DNe HCV 2005-A (or CV 1) and HCV 2005-B.

name	x	y	NUV	Δ NUV
HCV 2005-A	744.462	722.678	18.913	0.031
HCV 2005-B	771.660	1180.19	21.361	0.051

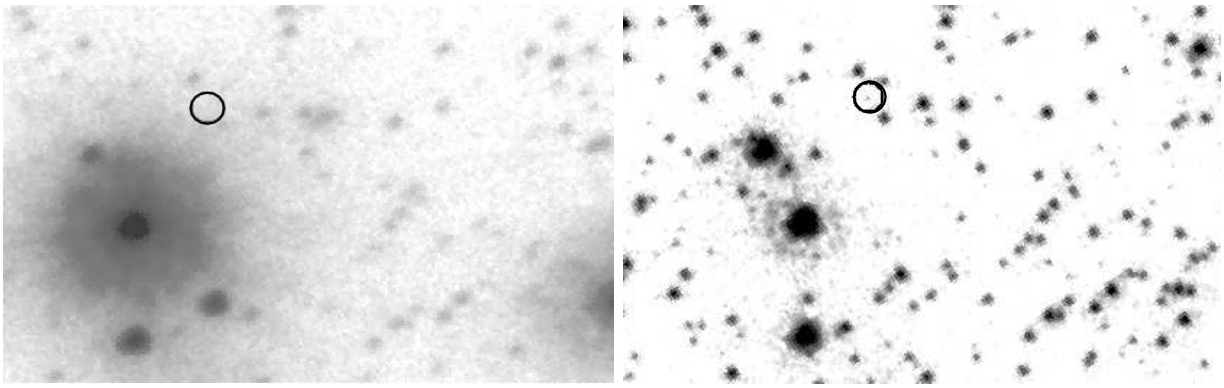

Fig. 14.— Same as Fig. 13, but for the DN HCV 2005-B. North is to the top left and east to the bottom left. HCV 2005-B appears as a faint NUV source (right), but is too faint to be detected in our FUV data (left).The field of view of these close-ups is $\approx 4\farcs5 \times 3''$. The location of HCV 2005-B in our image is at $\alpha = 21^h29^m58.226^s$, $\delta = 12°10'11\farcs4$.

Table 7: Number of gap sources and WD and BS candidates detected in GC. The cluster metallicity and the logarithmic core relaxation time log(tc) and halfmass relaxation time log(th) are taken from Harris (1996).

name	gap	WDs	BS	[Fe/H]	lg(tc)	lg(th)
NGC 2808	60	40	61	-1.15	8.30	9.13
M 15	57	28	69	-2.26	7.02	9.35